Ocean Modelling 87 (2015) 1–19

Contents lists available at ScienceDirect

Ocean Modelling

journal homepage: www.elsevier.com/locate/ocemod

# Dynamically consistent parameterization of mesoscale eddies. Part I: Simple model

Pavel Berloff *

*Department of Mathematics, Imperial College London, London, United Kingdom*

ARTICLE INFO

*Article history:*
Received 24 July 2014
Received in revised form 24 November 2014
Accepted 2 December 2014
Available online 17 January 2015

*Keywords:*
Geophysical fluid dynamics
Parameterization of mesoscale eddies

ABSTRACT

This work aims at developing a framework for dynamically consistent parameterization of mesoscale eddy effects for use in non-eddy-resolving ocean circulation models. The proposed eddy parameterization framework is successfully tested on the classical, wind-driven double-gyre model, which is solved both with explicitly resolved vigorous eddy field and in the non-eddy-resolving configuration with the eddy parameterization replacing the eddy effects. The parameterization locally approximates transient eddy flux divergence by spatially localized and temporally periodic forcing, referred to as the *plunger*, and focuses on the linear-dynamics flow solution induced by it. The nonlinear self-interaction of this solution, referred to as the *footprint*, characterizes and quantifies the induced cumulative eddy forcing exerted on the large-scale flow. We find that spatial pattern and amplitude of the footprint strongly depend on the underlying large-scale and the corresponding relationships provide the basis for the eddy parameterization and its closure on the large-scale flow properties. Dependencies of the footprints on other important parameters of the problem are also systematically analyzed. The parameterization utilizes the local large-scale flow information, constructs and scales the corresponding footprints, and then sums them up over the gyres to produce the resulting eddy forcing field, which is interactively added to the model as an extra forcing. The parameterization framework is implemented in the simplest way, but it provides a systematic strategy for improving the implementation algorithm.



## 1. Introduction

Mesoscale oceanic eddies populate nearly all parts of the global ocean and play important roles in maintaining the oceanic general circulation (e.g., McWilliams (2008)). The most straightforward, but also the most computationally intensive and, thus, unfeasible, way of accounting for the eddy effects on the large-scale circulation is resolving them dynamically with eddy-resolving ocean general circulation models (GCMs). This brute-force approach requires the computational grid resolution of about 1 km, which makes it feasible only for relatively short-time simulations, whereas the Earth system and climate change modeling routinely require much longer simulations over centuries and millenia. The only way to afford these time scales, while simulating the ocean in qualitatively correct way, is to *parameterize* the important eddy effects with simple and affordable but still accurate models embedded in the GCMs. In this context an eddy parameterization is a parametric mathematical model to be used in some coarse-grained, reduced-dynamics ocean circulation model. Ideally, the parameters involved are to be related to the explicitly resolved, large-scale circulation properties, thus, resulting in a turbulence closure for the eddies. Over the last few decades, the search for suitable eddy parameterizations remains a challenging theoretical topic with clear practical dimension.

In this paper, we propose, investigate and test a novel eddy parameterization framework that can stimulate both theoretical and practical advances. The main essence of the new parameterization is its focus on the *transient fluctuations* of the geostrophic eddy fluxes affecting the large-scale flow. The other essence is the dynamical consistency of the proposed framework. We aim more at the conceptual and dynamical foundation for the parameterization, rather than at the development of its final and polished algorithm. Overall, our results are fundamental, encouraging in terms of successful tests of the simplest initial implementation, and providing the framework for further systematic research and improvements.

Plan of the presentation is the following. In Section 1.1 we discuss the underlying philosophy and the background literature, as well as the implemented research strategy. The dynamical ocean model in which the parameterization is implemented and tested

* Address: Imperial College London, Department of Mathematics, Huxley Bldg., London SW7 2AZ, United Kingdom.
*E-mail address:* p.berloff@imperial.ac.uk

http://dx.doi.org/10.1016/j.ocemod.2014.12.008
1463-5003/

is described in Section 1.2. The nonlinear eddy dynamics explicitly simulated by the eddy-resolving ocean model configuration is analyzed in Section 2. In Sections 3 and 4 we study linear-dynamics flow responses to localized transient forcings, which imitate the actual eddy flux divergences acting on the large-scale flow, and find their dependencies on the large-scale flow. These analyses provide the theoretical underpinnings and principles of the eddy parameterization, which is eventually implemented and tested in Section 5. In Section 6 we summarize the parameterization framework, discuss the results and outline further research avenues.

### 1.1. Background and statement of the problem

The most common approach for parameterizing mesoscale eddy effects is (turbulent) *eddy diffusion*, which assumes that the eddies transport the corresponding flow property down its large-scale gradient. The eddy viscosity[1] is implemented in any GCM, and the eddy buoyancy diffusion, which parameterizes ubiquitous baroclinic instability processes (Gent and McWilliams, 1990), is used in most of the GCMs. The latter parameterization leads to substantial model improvements in many parts of the global ocean, especially in the Southern Ocean. Most of the diffusive parameterization theories focus on estimating various eddy diffusivity coefficients and relating them to the large-scale flow properties; for example, by invoking local linear-stability analysis (e.g., Eden (2011)) or by enforcing consistency with the physical conservation laws (e.g., Marshall et al. (2012), Ivchenko et al. (2013)). Very few studies attempt to challenge the very nature of the diffusive approach.

The main drawbacks of the diffusive approach are the following. First, the down-gradient assumption is often valid, especially for passive tracers, but it completely breaks down in the "negative eddy viscosity" and "negative eddy diffusivity" situations (Starr, 1968) occurring with active tracers, such as momentum, buoyancy and potential vorticity (PV). For example, in the eastward jet extension of the western boundary currents, the eddies flux PV up the large-scale PV gradient (Berloff et al., 2005b). Second, it is often assumed that the eddy diffusivity (and viscosity) coefficient is isopycnally isotropic and spatially homogeneous, although there is massive evidence against this assumption (e.g., Rypina et al. (2012)). Third, it is not usually understood how to relate an eddy diffusivity to the large-scale flow, hence, the diffusive parameterization remains unclosed and, thus, incomplete.

Despite intrinsic limitations of the eddy diffusion parameterizations, it is popular not only due to its mathematical simplicity, but also due to the lack of alternative theoretical ideas. An emerging theoretical alternative to the diffusion is to rely on *random* rather than deterministic representation of the diverging eddy fluxes. The main potential advantage of this approach is its capability to account for the negative-diffusivity eddy effects, which can not be modeled as diffusion due to the mathematical ill-posedness. In this case the randomness is justified by the observed, highly transient and structurally complicated pattern of the eddy fluxes. Although detailed observations of the oceanic eddy fluxes are problematic and scarce, the eddy-resolving GCMs robustly simulate the eddy flux divergence characterized by complex spatio-temporal patterns and by large transient fluctuations around small time-mean values (e.g., Li and von Storch (2013)). Can fluctuations of the eddy flux divergence be modeled as a random-forcing process, and can this approach eventually parameterize the important eddy effects? The foregoing, classical homogeneous-turbulence approach suggests to replace small-scale spectral nonlinear interactions by a statistically similar random forcing (e.g., Herring (1996)). The oceanic mesoscale turbulence is spatially inhomogeneous, therefore, the spectral approach should be reformulated in the physical space. However, this will not mitigate the main problems of the whole approach: (1) constraining random forcing with some physical principles and (2) relating parameters of the random forcing to the large-scale flow fields. Presumably, random forcing could be calibrated from the eddy-resolving simulations (e.g., Berloff et al. (2005a,b)) or estimated from the observations (assuming that we know what and where to observe). The other problem is (3) finding a proper large-scale circulation model compatible with the random forcing. Suggestions for such a model range from linear (e.g., see review by Penland (2007)) to nonlinear (Berloff et al., 2005a; Porta Mana and Zanna, 2014; Jansen and Held, 2014), depending on the objectives. In general the underlying model has to be fluid-dynamical and non-eddy-resolving, but severely truncated dynamics can be also used for specific purposes, such as modeling the large-scale low-frequency variability (e.g., Kravtsov et al. (2005)).

There are several precursors to the present work that involve both oceanic gyres and random-forcing approach. The first precursor is a sequence of papers (Berloff et al., 2005a,b; Berloff et al., 2007), in which the eddy-resolving solutions are used for constructing and constraining a family of random-forcing parameterizations incorporated in the non-eddy-resolving models and successfully tested. Nevertheless, the proposed framework has two shortcomings. First, relations between the random forcing and the large-scale flow properties remain poorly understood, thus, hampering the complete closure. Second, the randomly forced flow dynamics remains poorly understood, thus, hampering the physical understanding. The second precursor to our work is recent study by Porta Mana and Zanna (2014), in which the random forcing is shaped by the probability density function calibrated on the eddy-resolving simulations and conditioned on the explicitly resolved large-scale flow properties. Our present work compliments and extends the above-described studies. It is novel in the sense that, not only it illuminates the dynamical connections between transient eddies and their large-scale effects, but also it develops and implements the corresponding eddy parameterization.

The central building block of our approach is analysis of the linear-dynamics responses to spatially localized and temporally periodic forcing function referred to as *plunger* as representing an elementary transient action by the eddies. Flow response to a plunger can be treated as the convolution of the Green's functions of the problem. The temporal periodicity of the plunger is an interim simplification that can be later upgraded to more general, random but time-correlated process (e.g., Berloff and McWilliams (2003)). The proposed approach is radically different from the classical spectral random forcing, because spatially localized forcing is spectrally broad-band, with phase-correlated harmonics.

The simplest conceptual model of the nonlinear rectification of plunger-induced flows is sometimes referred to as the "beta-plane plunger", and its main aspect is emergence of (1) a rectified eastward jet at the directly forced latitudes and (2) westward return currents outside of them (Whitehead, 1975; Haidvogel and Rhines, 1983; Waterman and Jayne, 2011; Waterman and Jayne, 2012). The eastward/westward flows are driven by the diverging upgradient/downgradient eddy PV fluxes, and in this process both the nonlinearity and the background PV gradient are fundamentally important. In the simplest set-up, the background PV gradient is uniform and set by the beta-plane approximation. In this paper we systematically explore the plunger dynamics before incorporating it into the parameterization.

Our approach is the following. We resorted to the quasigeostrophic (QG) dynamics of the classical double-gyre model, which is solved both in the eddy-resolving and non-eddy-resolving con-

[1] Here, the term "viscosity" applies to the momentum, and the term "diffusivity" applies to all other scalar properties.

figurations, with relatively large and small Reynolds numbers, respectively. First, we diagnosed the eddy PV flux divergence of the reference eddy-resolving solution and treated its history as the nonlinear eddy forcing acting on the large-scale circulation. Subsequent statistical analysis of the eddy forcing provided us with the characteristic length and time scales for use in the forthcoming parameterization. The time-mean component of the reference solution provided us with the benchmark for assessing quality of the parameterization: a non-eddy-resolving model with properly parameterized eddy effects must be able to reproduce the benchmark. Second, we systematically studied the linear-dynamics plunger solutions and their dependencies on the underlying large-scale flow and other physical parameters. For each solution we analyzed its nonlinear self-interaction, referred to as the *footprint* and describing the feedback on the large-scale flow. The footprint dependencies on the large-scale flow provided us with the parameterization closure. Finally, we implemented the parameterization in the non-eddy-resolving model, successfully tested the outcome against the benchmark, and discussed further avenues for the parameterization improvement.

### 1.2. Dynamical ocean model

A dynamical model required by our study must operate at relatively large Reynolds number and resolve many eddy scales. The QG dynamics is our obvious choice, because it is not only by 2–3 orders of magnitude computationally faster than the analogous primitive equations, but also more transparent to mathematical analyses. In the classical double-gyre configuration, the model represents idealized, wind-driven midlatitude ocean circulation. It describes a flat-bottom square basin with the north–south and east–west boundaries, and with prescribed density stratification. The dynamics is governed by the QG PV equations for 3 stacked isopycnal layers:

$$\frac{\partial q_1}{\partial t} + J(\psi_1, q_1) + \beta \frac{\partial \psi_1}{\partial x} = \frac{1}{\rho_1 H_1} W + \nu \nabla^4 \psi_1, \tag{1}$$

$$\frac{\partial q_2}{\partial t} + J(\psi_2, q_2) + \beta \frac{\partial \psi_2}{\partial x} = \nu \nabla^4 \psi_2, \tag{2}$$

$$\frac{\partial q_3}{\partial t} + J(\psi_3, q_3) + \beta \frac{\partial \psi_3}{\partial x} = -\gamma \nabla^2 \psi_3 + \nu \nabla^4 \psi_3, \tag{3}$$

where the layer index starts from the top; $J(,)$ is the Jacobian operator; $\rho_1 = 10^3\ \mathrm{kg\,m^{-3}}$ is the upper layer density; $\beta = 2 \times 10^{-11}\ \mathrm{m^{-1}\,s^{-1}}$ is the planetary vorticity gradient; $\nu = 20\ \mathrm{m^2\,s^{-1}}$ is the eddy viscosity coefficient in the eddy-resolving model configuration; and $\gamma = 4 \times 10^{-8}\ \mathrm{s^{-1}}$ is the bottom friction parameter (corresponding to the spin-down time of about 290 days). The basin size is $2L = 3840$ km, so that $-L \leqslant x \leqslant L$, and $-L \leqslant y \leqslant L$. The isopycnal layer depths are $H_1$=250, $H_2$=750, and $H_3$=3000 m. The PV anomalies $q_i$ and the velocity streamfunctions, $\psi_i$, are related as

$$q_1 = \nabla^2 \psi_1 + S_1(\psi_2 - \psi_1), \tag{4}$$

$$q_2 = \nabla^2 \psi_2 + S_{21}(\psi_1 - \psi_2) + S_{22}(\psi_3 - \psi_2), \tag{5}$$

$$q_3 = \nabla^2 \psi_3 + S_3(\psi_2 - \psi_3), \tag{6}$$

where the stratification parameters are

$$S_1 = \frac{f_0^2}{H_1 g_1'}, \quad S_{21} = \frac{f_0^2}{H_2 g_1'}, \quad S_{22} = \frac{f_0^2}{H_2 g_2'}, \quad S_3 = \frac{f_0^2}{H_3 g_2'}, \tag{7}$$

$g_1'$ and $g_2'$ are the reduced gravities, associated with the density jumps across the upper and lower, respectively, internal interfaces between the isopycnal layers, and $f_0 = 0.83 \times 10^{-4}\ \mathrm{s^{-1}}$ is the Coriolis parameter. The stratification parameters are chosen so that the first and second Rossby deformation radii are $Rd_1 = 40$ km and $Rd_2 = 20.6$ km, respectively.

The double-gyre Ekman pumping $W(x, y)$ is asymmetric in order to avoid artificial symmetrization of the gyres:

$$W(x, y) = -\frac{\pi \tau_0 A}{L} \sin\left[\frac{\pi(L + y)}{L + Bx}\right], \quad y \leqslant Bx, \tag{8}$$

$$W(x, y) = +\frac{\pi \tau_0}{LA} \sin\left[\frac{\pi(y - Bx)}{L - Bx}\right], \quad y > Bx, \tag{9}$$

where the asymmetry parameter is $A = 0.9$, the non-zonal tilt parameter is $B = 0.2$, and the wind stress amplitude is $\tau_0 = 0.8\ \mathrm{N\,m^{-2}}$. The eddy-resolving model operates at a large Reynolds number defined as

$$Re = \frac{U\,2L}{\nu} = \frac{\tau_0}{\rho_1 H_1 \beta \nu} \approx 800, \tag{10}$$

where $U = \tau_0 (\rho_1 H_1 2L\,\beta)^{-1} = 0.0417\ \mathrm{m\,s^{-1}}$ is the upper-ocean Sverdrup velocity scale. The partial-slip condition, which involves derivatives in the normal direction to the boundary,

$$\alpha \frac{\partial^2 \psi_i}{\partial n^2} - \frac{\partial \psi_i}{\partial n} = 0, \tag{11}$$

is applied on the lateral walls, and the parameter $\alpha = 120$ km can be interpreted as the boundary sublayer length scale. The mass conservation constraints are also imposed:

$$\frac{\partial}{\partial t} \iint (\psi_1 - \psi_2)\, dx\, dy = 0, \quad \frac{\partial}{\partial t} \iint (\psi_2 - \psi_3)\, dx\, dy = 0. \tag{12}$$

The model is solved by the high-resolution numerical algorithm described in Karabasov et al. (2009), on the uniform $513^2$ grid with 7.5 km nominal resolution.

More simple, doubly periodic two- and three-layer configurations of the model (Berloff et al., 2011) are also used for the plunger-driven solutions with the period equal to the basin size. The computational domains are of the same size as the closed basin. The three-layer stratification is the same as in the double-gyre model. In the two-layer case, the upper and deep layer thicknesses are $H_1 = 1$ km and $H_2 = 3$ km, respectively, and the reduced-gravity coefficient $g_1'$ is such that the first baroclinic Rossby deformation radius,

$$Rd_1 = g_1' \frac{\sqrt{H_1 H_2}}{f_0 \sqrt{H_1 + H_2}}, \tag{13}$$

is 40 km, as in the three-layer model, and the two-layer stratification parameters are

$$S_1 = \frac{f_0^2}{H_1 g_1'}, \quad S_2 = \frac{f_0^2}{H_2 g_1'}. \tag{14}$$

The two-layer governing equations,

$$\frac{\partial q_1}{\partial t} + J(\psi_1, q_1) + \beta \frac{\partial \psi_1}{\partial x} = \nu \nabla^4 \psi_1, \tag{15}$$

$$\frac{\partial q_2}{\partial t} + J(\psi_2, q_2) + \beta \frac{\partial \psi_2}{\partial x} = \nu \nabla^4 \psi_2 - \gamma \nabla^2 \psi_2, \tag{16}$$

are combined with the relations between the PV anomalies and velocity streamfunctions,

$$q_1 = \nabla^2 \psi_1 + S_1(\psi_2 - \psi_1), \tag{17}$$

$$q_2 = \nabla^2 \psi_2 + S_2(\psi_1 - \psi_2) \tag{18}$$

and the imposed mass constraint. Forcing in the governing equations is provided by the background, vertically sheared zonal flow with velocity $U_i$, so that:

$$\psi_i \longrightarrow -U_i y + \psi_i, \tag{19}$$

The doubly periodic models are on $512^2$ uniform grid by the Fourier transforms (Section 4).

## 2. Statistical analysis of the eddying gyres

In this section we discuss the benchmark eddy-resolving solution of the gyres and its transient eddy forcing. The flow solution is characterized by vigorous eddy field evolving on the underlying large-scale gyres separated by the intense and meandering eastward jet extension of the western boundary currents (Fig. 1). In the upper ocean the eastward jet is characterized by the sharp cross-jet PV gradient and the strongest eddy activity; and in the deep ocean the jet is characterized by nearly homogenized pool of PV maintained by the eddy stirring. The eastward jet with its adjacent recirculation zones is an important flow feature that controls the oceanic meridional transport. The jet is notoriously difficult to get parameterized by diffusion, because it is maintained by anti-diffusive cross-jet eddy PV fluxes associated with the eddy backscatter (Berloff et al., 2005a,b; Waterman and Jayne, 2011; Waterman and Jayne, 2012), rather than by diffusive eddy stirring on the jet flanks, as it typically happens in zonally symmetric jets (e.g., Dritschel and McIntyre (2008)).

In the quasigeostrophic framework, the eddy effects on the large-scale flow can be quantified by convergence of the eddy PV flux, which consists of the fluxes of relative vorticity,

$$R_i = \nabla^2 \psi_i \tag{20}$$

and isopycnal stretching (i.e., buoyancy anomaly), which in the three-layer case is given by

$$B_1 = S_1(\psi_2 - \psi_1), \quad B_2 = S_{21}(\psi_1 - \psi_2) + S_{22}(\psi_3 - \psi_2),$$
$$B_3 = S_3(\psi_2 - \psi_3). \tag{21}$$

Each eddy flux is found by decomposing the flow solution into the time-mean (indicated by overbar) and transient components. The resulting eddy forcing,

$$F_i(t,x,y) \equiv -[\nabla \cdot \mathbf{u}_i q_i - \nabla \cdot \overline{\mathbf{u}_i q_i}] \tag{22}$$

is interpreted as the internally generated eddy PV forcing. It can be further decomposed into the Reynolds stress and form stress components, consistent with (20) and (21). Next, $F_i$ can be decomposed into the time-mean $\bar{F}_i(x,y)$ and the transient $F_i'(t,x,y)$ components, and we find that the standard deviation of the transient component is larger than $\bar{F}_i$ by two orders of magnitude (Fig. 2). The dominance of the transient component is rarely noted in the literature (e.g., Berloff et al. (2005b), Li and von Storch (2013)), but it actually provides the main motivation for parameterizing the eddies in terms of random processes (e.g., Porta Mana and Zanna (2014)). The spatio-temporal structure of $F'$ is complex, and this complexity becomes more evident, when $F'$ is normalized by its standard deviation (Fig. 3).

We simplified the statistical analysis of the transient eddy forcing by focusing on its upper-ocean component $F_1'(t,x,y)$, because its standard deviation dominates over the deep-ocean one, and it plays the key role in maintaining the eastward jet (Berloff et al., 2005a). We sampled history of $F_1'$ and applied 60 by 60 km running-average spatial filtering, as well as the 20-day running-average temporal filtering, in order to coarse-grain the field. The choice of filtering is subjective, but we checked that the outcome is not very sensitive to it. For the purposes of this study, we need only qualitative estimates of the eddy forcing properties, but note that the coarse-graining can be optimized and even dynamically

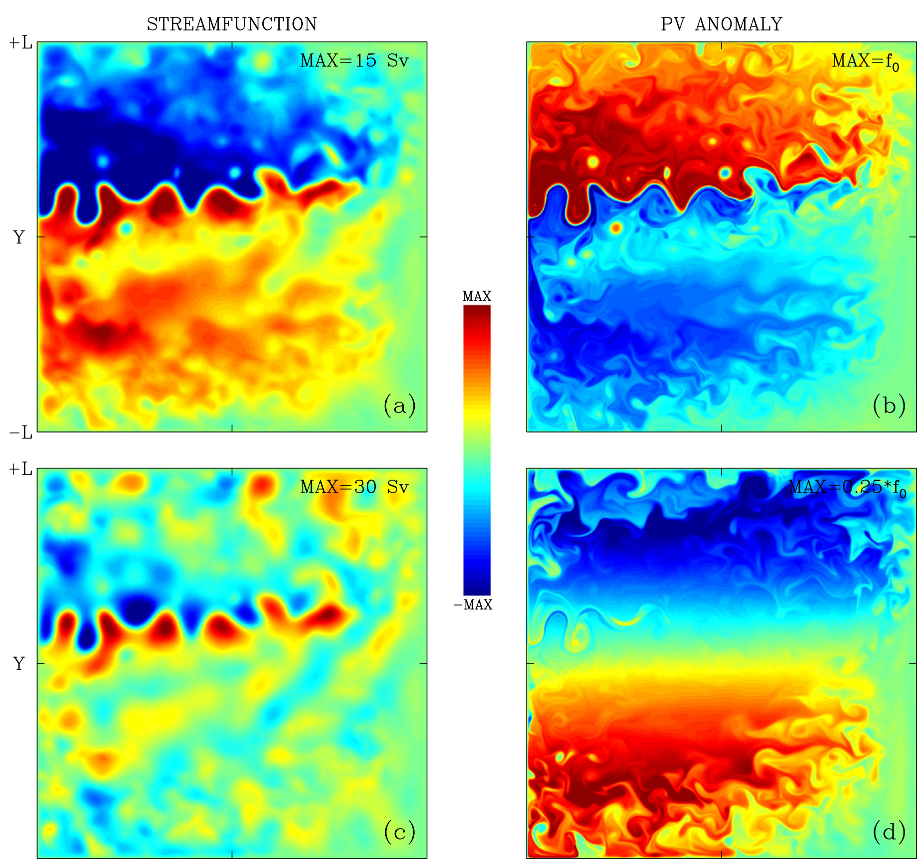


**Fig. 1.** Snapshot of the eddy-resolving double-gyre circulation. Upper/lower panels correspond to the upper/middle isopycnal layer; left and right panels show transport streamfunction and PV anomalies, respectively. The most energetic eddies are concentrated around the eastward jet and maintain it through the nonlinear rectification (i.e., eddy backscatter). Color scale range is indicated in each panel: the streamfunction units are Sverdrups (Sv), and the PV anomaly units are $f_0$.

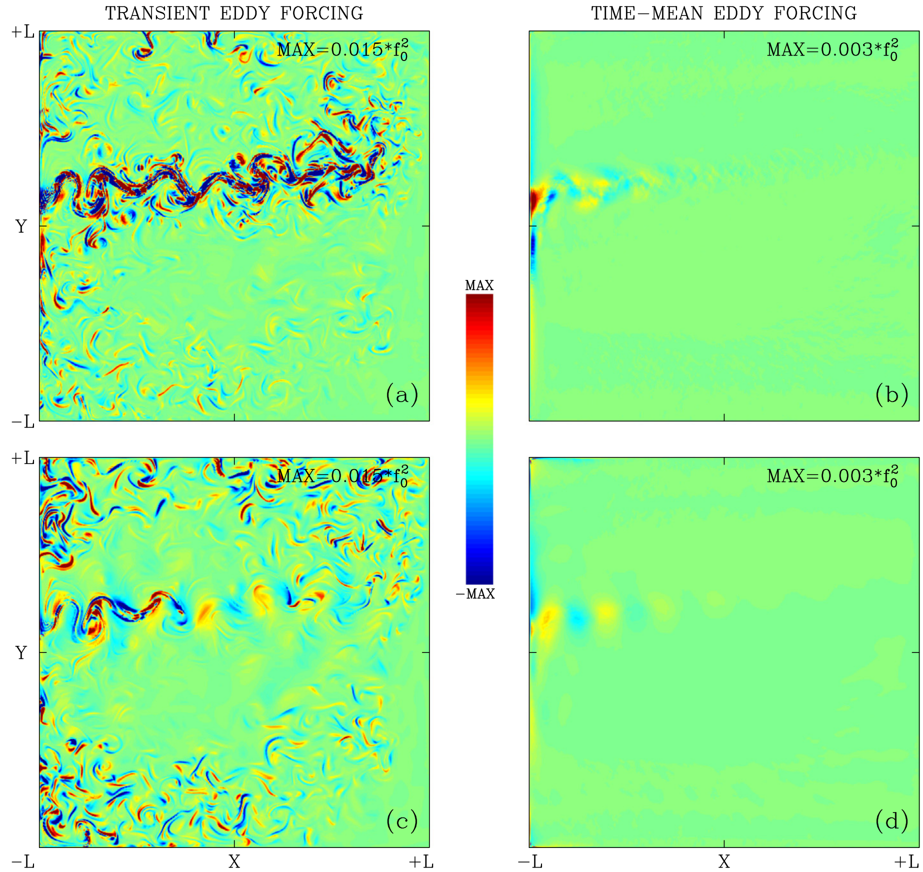


**Fig. 2.** Instantaneous and time-mean patterns of the double-gyre eddy forcing. Upper/lower panels correspond to the upper/middle isopycnal layer; left panels show instantaneous (transient) fluctuations of the eddy forcing corresponding to the flow snapshot in Fig. 1; right panels show the time-mean component of the eddy forcing. The fluctuations completely dominate over the time-mean component, and even more so in the eastward-jet region and in the upper ocean. Color scale range is indicated in each panel (units are $f_0^2$).

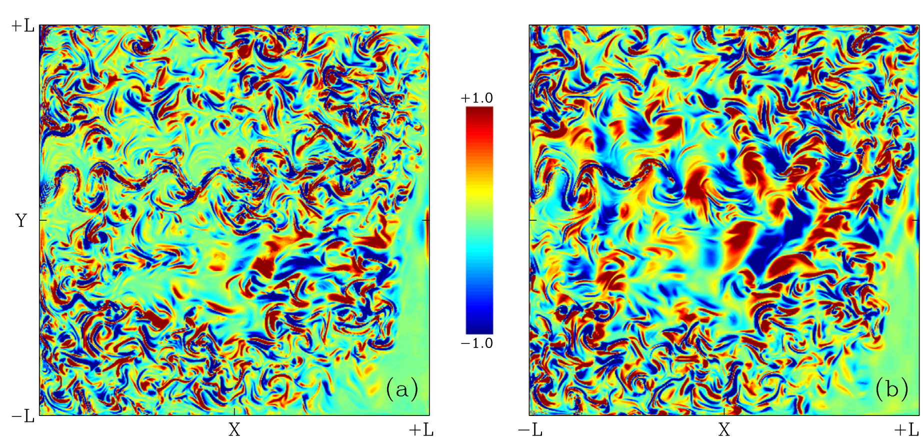


**Fig. 3.** Instantaneous pattern of the transient eddy forcing normalized by the standard deviation. (a) Upper-ocean and (b) deep-ocean patterns correspond to those in Figs. 2a and 2c, respectively. The patterns are characterized by larger length scales seen in the deep ocean and in the eastern part of the upper-ocean subtropical gyre; and around the upper-ocean eastward jet the length scales are more uniform.

constrained (Berloff et al., 2005b). The simplest starting point for analyzing $F'$ is estimating its spatial and temporal correlations (e.g., Berloff et al. (2005a)). From the correlation functions, estimates of the correlation length and time scales can be made at every location, but we chose a simpler approach by sampling the correlations at 25 reference sites that cover the main area of the eddy activity. These sites not only cover the eastward jet and its adjacent recirculations zones but also extend into the gyre interiors and western boundary currents (Fig. 4).

For each sampling site $(x_j, y_j)$, $j = 1, \ldots, 25$, the correlation length scale was found by considering correlations between $F'_1(t, x_j, y_j)$ and $F'_1(t, x, y)$, both normalized by their standard deviations. In the neighborhood of $(x_j, y_j)$ with radius of 100 km, we counted the number of grid points with the correlation values larger than 0.1 and obtained the area corresponding to large and positive correlations. The correlation radius $r_{corr}(x_j, y_j)$ is found as the radius of the circle with the same area, and to large degree the values of $r_{corr}$ are spatially uniform and about 50–60 km (Table 1). In

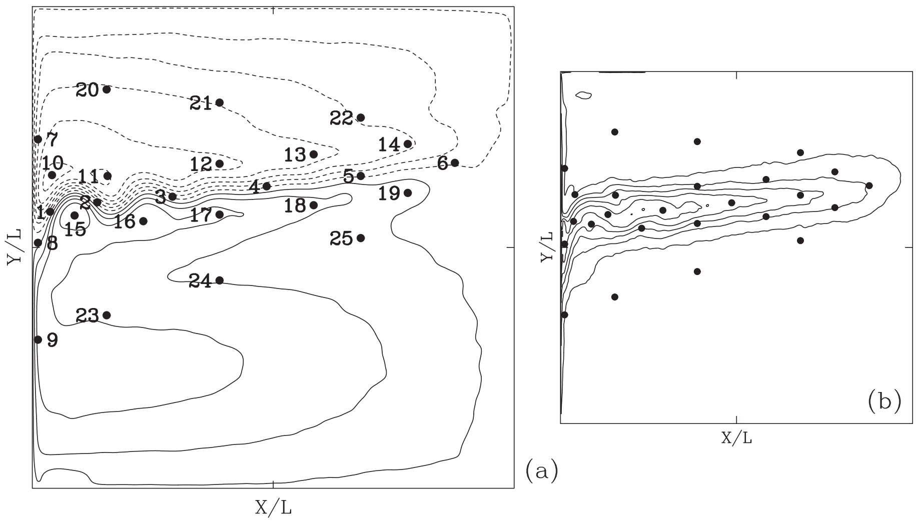


**Fig. 4.** Reference sites for obtaining the detailed diagnostics of the eddy forcing. (a) Time-mean upper-ocean velocity streamfunction of the eddy-resolving solution (CI = 4 Sv) and the numbered reference sites; (b) standard deviation of the upper-ocean eddy forcing (CI = $0.005f_0^2$) and the reference sites.

the following analyses we consider circular plungers with radius $r_0 = r_{corr} = 60$ km, but variations of $r_0$ are also explored. We also analyzed the time series of $F_1'(t, x_0, y_0)$, estimated their median frequencies and found that they mostly remain within the range corresponding to periods of 60–70 days (Table 1). For simplicity, in the following analyses we focus on plunger time period $T = 65$ days, but variations of $T$ are also explored.

The parameterization further below locally relates eddy forcing to the underlying large-scale flow, and for initial simplicity, only zonal component of the large-scale flow is accounted for. Additional interim simplification to be used in the parameterization is simple empirical relationship between large-scale zonal isopycnal velocities. Mutual scatterplots between the time-mean velocities $\bar{u}_i(x, y),\ i = 1, 3$, (Fig. 5) show that there is no simple global relationship between them, but there is a local approximate relationship around the eastward jet extension and its adjacent recirculation zones (in cm s$^{-1}$):

$$\bar{u}_2 = -2.1 + 0.5\bar{u}_1, \quad \bar{u}_3 = -2.8 + 0.2\bar{u}_1. \tag{23}$$

In the following sections we use (23) to simplify the analyses and the parameterization closure.

## 3. Solutions for simple plungers

In this section we explain how to solve for the linear flow responses to spatially localized and time-dependent forcing functions, referred to as *plungers*, and in Section 4 we discuss properties of these solutions.

The elementary plunger is represented by a $\delta$-function in space and harmonic oscillation in time; and the corresponding flow solution is the Green's function of the problem. More realistic plunger is spatially distributed and broad-band in the frequency domain, and the corresponding flow solution can be obtained as the convolution of the involved Green's functions.

As the starting point, let us consider the conservative equivalent-barotropic dynamics linearized around the state of rest and driven by the elementary $\delta$-plunger with frequency $\omega_0$, so that:

$$\frac{\partial}{\partial t}\left(\nabla^2\psi - S\psi\right) + \beta\frac{\partial\psi}{\partial x} = \delta(\mathbf{x})e^{-i\omega_0 t}, \tag{24}$$

where $S^{-1/2}$ is the Rossby deformation radius. Solution of this equation is the Green's function $G(t, x, y)$, that can be written as

$$G = \tilde{G}e^{iAx}e^{-i\omega_0 t}, \tag{25}$$

so that the second exponent accounts for the time dependence, and the first exponent allows to get rid of the $\partial/\partial x$ term in (24) (see Haidvogel and Rhines (1983)). Since

$$\frac{\partial G}{\partial x} = \left(\frac{\partial\tilde{G}}{\partial x} + iA\tilde{G}\right)e^{iAx}, \quad \frac{\partial^2 G}{\partial x^2} = \left(\frac{\partial^2\tilde{G}}{\partial x^2} + 2iA\frac{\partial\tilde{G}}{\partial x} - A^2\tilde{G}\right)e^{iAx}, \tag{26}$$

these equations and (25) are used to rewrite (24) as

$$\nabla^2\tilde{G} + \left[2iA + \frac{i\beta}{\omega_0}\right]\frac{\partial\tilde{G}}{\partial x} + \left[-\frac{\beta A}{\omega_0} - A^2 - S\right]\tilde{G} = \frac{i}{\omega_0}\delta(\mathbf{x}). \tag{27}$$

Let us choose $A = -\beta/(2\omega_0)$ and obtain:

$$G = \tilde{G}\exp\left\{-i\left(\frac{\beta x}{2\omega_0} + \omega_0 t\right)\right\}, \quad \nabla^2\tilde{G} + \left[\left(\frac{\beta}{2\omega_0}\right)^2 - S\right]\tilde{G} = \frac{i}{\omega_0}\delta(\mathbf{x}). \tag{28}$$

Solution for $\tilde{G}$ can be formulated in terms of the Hankel function of the second kind $H_0^{(2)}$, therefore:

$$G(t, x, y) \sim H_0^{(2)}(\gamma r)\exp\left\{-i\left(\frac{\beta x}{2\omega_0} + \omega_0 t\right)\right\}, \quad \gamma^2 \equiv \left(\frac{\beta}{2\omega_0}\right)^2 - S. \tag{29}$$

**Table 1**
Eddy forcing correlation length and time scales estimated at the reference locations.

| | 1 | 2 | 3 | 4 | 5 | 6 | 7 | 8 | 9 | 10 | 11 | 12 | 13 | 14 | 15 | 16 | 17 | 18 | 19 | 20 | 21 | 22 | 23 | 24 | 25 |
|---|---|---|---|---|---|---|---|---|---|---|---|---|---|---|---|---|---|---|---|---|---|---|---|---|---|
| Period (days) | 61 | 66 | 66 | 68 | 65 | 68 | 62 | 66 | 61 | 69 | 65 | 58 | 62 | 64 | 57 | 61 | 65 | 63 | 63 | 73 | 70 | 66 | 85 | 65 | 63 |
| Radius (km) | 61 | 56 | 54 | 55 | 56 | 54 | 52 | 60 | 45 | 54 | 56 | 55 | 57 | 56 | 50 | 53 | 54 | 52 | 53 | 63 | 63 | 57 | 58 | 67 | 52 |

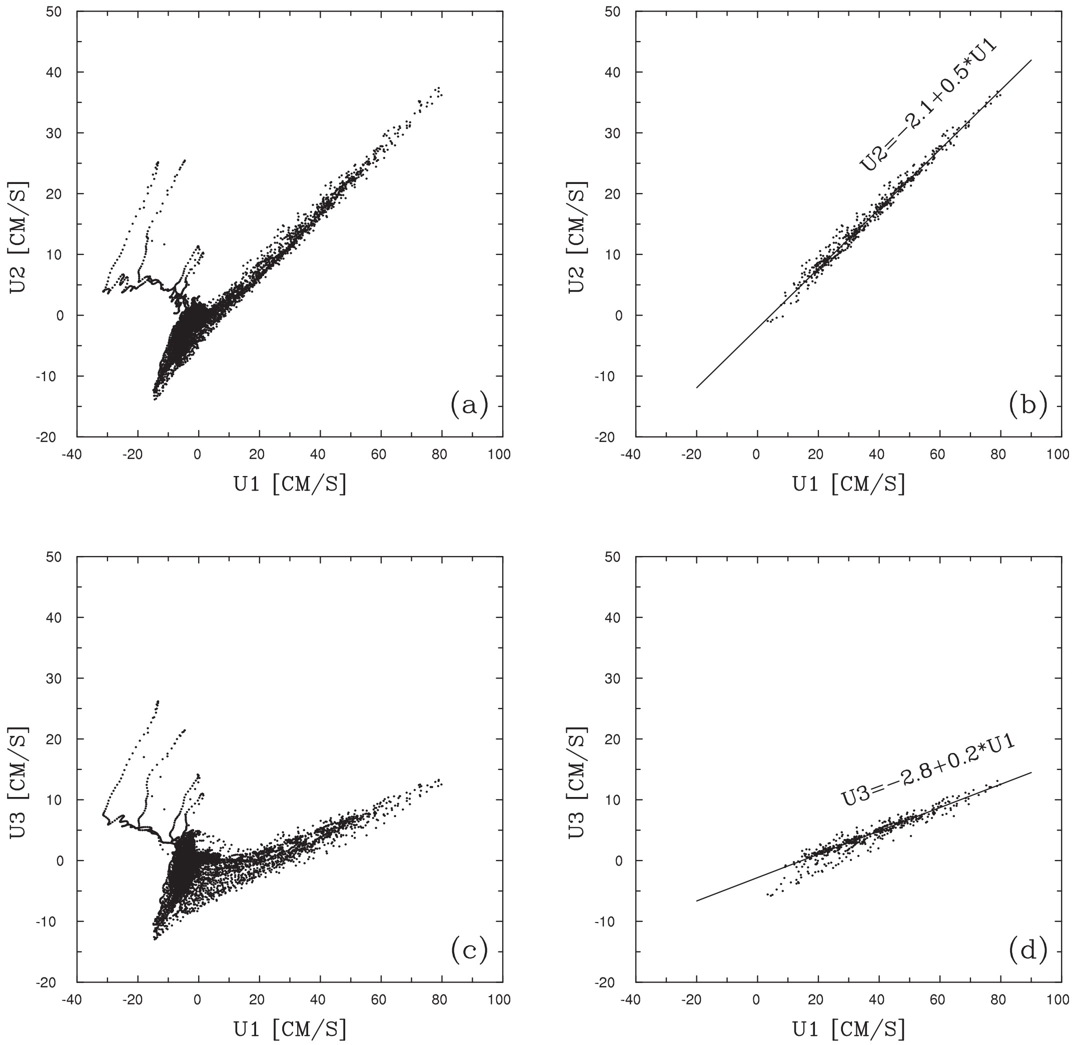


**Fig. 5.** Empirical relations between the time-mean zonal velocities of the eddy-resolving solution at different depths. Shown are the velocity scatterplots between the upper and middle layers (upper panels), and between the upper and bottom layers (lower panels). On the left panels the velocity values are taken uniformly, at every coarse-grid point; and on the right panels they are taken nonuniformly, only around the eastward jet region, in the locations where the absolute time-mean PV flux is large (more than $4 \times 10^{-8}$ m s$^{-2}$). On the right panels the linear least-squares fits are indicated by the straight lines and the corresponding relationships, that allow to express $\overline{u_2}$ and $\overline{u_3}$ as the linear functions of $\overline{u_1}$.

The Green's function (29) ceases to exist when $\gamma^2 < 0$, and this sets the maximum $\omega_0$ for which a radiating solution exists. In other words, waves can radiate when the forcing frequency is in the band of linear Rossby wave frequencies, and this sets the cutoff. For our values of $\beta$ and $Rd_1 = S^{-1/2}$ (40 km), this corresponds to the shortest forcing period of about 180 days. Note, that this is much longer than the median time scale of the double-gyre eddy forcing (Section 2 and Table 1), suggesting that purely baroclinic response to a plunger cannot radiate and must be trapped. On the contrary, purely barotropic response ($S = 0$) always radiates, because $\gamma$ is real. In Section 4 we show, that in the presence of a vertical background shear, the dynamical coupling between the baroclinic and barotropic motions allows baroclinic radiation.

In the two-layer linear QG model without background flow, the plunger dynamics is decoupled into separate equations for the barotropic and baroclinic vertical modes. The corresponding Green's functions are given by (29) with $S$ being zero and finite, respectively. In the presence of a vertically sheared background flow, the vertical modes are dynamically coupled. Analytic expression for the corresponding two-layer Green's function is unknown, but its numerical solution can be efficiently and accurately obtained by the Fourier transforms. Let us consider the two-layer linear dynamics with horizontally uniform zonal background flow given by $U_1$ and $U_2$, and with the plunger restricted to the upper layer. The governing equations analogous to (24) are:

$$\frac{\partial}{\partial t}\Big(\nabla^2\psi_1 - S_1(\psi_1 - \psi_2)\Big) + \beta_1\frac{\partial\psi_1}{\partial x} + U_1\frac{\partial}{\partial x}\Big(\nabla^2\psi_1 - S_1(\psi_1 - \psi_2)\Big) = \delta(\mathbf{x})e^{-i\omega_0 t}, \tag{30}$$

$$\frac{\partial}{\partial t}\Big(\nabla^2\psi_2 - S_2(\psi_2 - \psi_1)\Big) + \beta_2\frac{\partial\psi_2}{\partial x} + U_2\frac{\partial}{\partial x}\Big(\nabla^2\psi_2 - S_2(\psi_2 - \psi_1)\Big) = 0, \tag{31}$$

where $\beta_1 = \beta + S_1(U_1 - U_2)$ and $\beta_2 = \beta + S_2(U_2 - U_1)$ are the isopycnal background PV gradients. By substituting

$$G_1 = \tilde{G}_1 e^{-i\omega_0 t}, \quad G_2 = \tilde{G}_2 e^{-i\omega_0 t}, \tag{32}$$

the following system of equations is obtained:

$$-i\omega_0\Big(\nabla^2\tilde{G}_1 - S_1(\tilde{G}_1 - \tilde{G}_2)\Big) + \beta_1\frac{\partial\tilde{G}_1}{\partial x} + U_1\frac{\partial}{\partial x}\Big(\nabla^2\tilde{G}_1 - S_1(\tilde{G}_1 - \tilde{G}_2)\Big) = \delta(x)\delta(y), \tag{33}$$

$$-i\omega_0\Big(\nabla^2\tilde{G}_2 - S_2(\tilde{G}_2-\tilde{G}_1)\Big) + \beta_2\frac{\partial\tilde{G}_2}{\partial x} + U_2\frac{\partial}{\partial x}\Big(\nabla^2\tilde{G}_2 - S_2(\tilde{G}_2-\tilde{G}_1)\Big) = 0. \quad (34)$$

Let us assume that the Fourier transform of the solution exists:

$$\tilde{g}_1(k,l) = \iint \tilde{G}_1(x,y)e^{-i(kx+ly)}dx\,dy,$$
$$\tilde{g}_2(k,l) = \iint \tilde{G}_2(x,y)e^{-i(kx+ly)}dx\,dy. \quad (35)$$

Then, the Fourier transform of (33), (34) yields

$$-i(kU_1+\omega_0)\Big[-(k^2+l^2+S_1)\tilde{g}_1 + S_1\tilde{g}_2\Big] - i\beta_1 k\,\tilde{g}_1 = 1, \quad (36)$$

$$-i(kU_2+\omega_0)\Big[-(k^2+l^2+S_2)\tilde{g}_2 + S_2\tilde{g}_1\Big] - i\beta_2 k\,\tilde{g}_2 = 0 \quad (37)$$

and this can be rewritten as the system of two linear equations with nonzero rhs:

$$\Big[\beta_1 k - (kU_1+\omega_0)(k^2+l^2+S_1)\Big]\tilde{g}_1(k,l) + [S_1(kU_1+\omega_0)]\tilde{g}_2(k,l) = i, \quad (38)$$

$$[S_2(kU_2+\omega_0)]\tilde{g}_1(k,l) + \Big[\beta_2 k - (kU_2+\omega_0)(k^2+l^2+S_2)\Big]\tilde{g}_2(k,l) = 0. \quad (39)$$

If the external forcing has spatially distributed amplitude $F_1(x,y)$, then its Fourier transform $f_1(k,l)$ should multiply the rhs of (38). The final equations can be written in the matrix form:

$$\mathbf{A}\begin{pmatrix}\tilde{g}_1\\ \tilde{g}_2\end{pmatrix} \equiv \begin{pmatrix}a & b\\ c & d\end{pmatrix}\begin{pmatrix}\tilde{g}_1\\ \tilde{g}_2\end{pmatrix} = \begin{pmatrix}if_1\\ 0\end{pmatrix} \quad (40)$$

and for each $(k,l)$ the solution is given by Cramer's rule:

$$\tilde{g}_1(k,l) = i\frac{d\,f_1}{\det(\mathbf{A})}, \quad \tilde{g}_2(k,l) = -i\frac{c\,f_1}{\det(\mathbf{A})}. \quad (41)$$

The inverse Fourier transform and (32) provide the solution in the physical space. The three-layer extension of the above derivation, augmented by adding spatially distributed forcing function is presented in Appendix. This extension is also analyzed in Section 4, to be used in Section 5 for the ultimate parameterization of the double-gyre eddies.

The solutions obtained in this section in their general forms are considered in the next section in detail. Extension of the solutions to more general time dependencies is a straightforward convolution of the corresponding Green's functions, and, therefore, it is not discussed here. Extension of the solutions to more general background flows and boundary conditions is not straightforward, and, therefore, it is left out for a separate study.

## 4. Analysis of simple plungers

A plunger located at $(x_0,y_0)$ is formulated as

$$F(t,x,y;x_0,y_0) = 2.16A(t)\cos\left(\frac{\pi}{2}\frac{r}{r_0}\right), \quad r<r_0; \quad (42)$$

$$F(t,x,y;x_0,y_0) = 0, \quad r \geqslant r_0, \quad (43)$$

where $r=\sqrt{(x-x_0)^2+(y-y_0)^2}$ is the distance from the center, and the forcing is concentrated within radius $r_0$. Our motivation for the radial dependence in (42) is to have a smooth and monotonic decay over the radius representing the correlation length scale. Our simple initial choice can be straightforwardly upgraded to a more realistic approximation of the transient eddy forcing. We also assumed that the area integral of the cosine forcing within the circle is equal to the unity, and this yielded the geometric factor of 2.16 in (42). The amplitude is chosen $A(t)\sim\cos(2\pi t/T)$, and its magnitude is the same for all linear solutions considered. Both $r_0$ and $T$ are eventually fixed as the length and time scales of the eddy forcing from the eddy-resolving reference solution (Section 2), but in this section we study solution dependencies on them. Note, that the instantaneous basin-averaged PV injected by a plunger given by (42), (43) is nonzero. We checked whether this matters by introducing small, spatially uniform correction that brings the basin-averaged instantaneous PV to zero. This correction results in negligible changes of the solution, therefore, it is further neglected.

We considered two-layer linear dynamics in the doubly periodic domain (Section 3) and obtained the solutions for a set of background flows with $-20<U_1<60$ cm s$^{-1}$ (with 1 cm s$^{-1}$ interval) and $U_2=0$. Some typical solutions are shown in Fig. 6. In the absence of the background flow (Fig. 6c), the solution is completely decoupled (as discussed in Section 3) into the barotropic- and baroclinic-mode patterns defined here as

$$\phi_1 = \frac{H_1}{H_1+H_2}\psi_1 + \frac{H_2}{H_1+H_2}\psi_2, \quad \phi_2=\psi_1-\psi_2. \quad (44)$$

In this case, in accord with (29) the barotropic mode radiates away, whereas the baroclinic mode remains trapped in the forced region $r<r_0$. Since the solutions are found in the doubly periodic domain, there is significant interference of the waves radiated by the periodic copies of the main plunger. This interference is manifested by complicated real and imaginary spatial patterns of the solutions, as well as by the corresponding complex amplitudes (Fig. 6). To understand this interference, we studied spin-up adjustments of the solutions by integrating the time-dependent governing equations (by the same numerical algorithm as in the double-gyre model) and observing how the interference patterns emerge from the individual waves that emerge, radiate and interact (not shown). In the presence of the background shear, the barotropic and baroclinic modes are dynamically coupled, therefore, the baroclinic part of the solution escapes from the trap and radiates away. We refer to this phenomenon as the *baroclinic delocalization* and argue, that this is the main mechanism for overcoming the baroclinic trapping set by (29).

The other significant background-flow effects are positive correlation between the amplitudes of the background shear and the baroclinic mode, and dependence of the spatial solution patterns on the background flow. Some solutions are characterized by the distinct trains of eddies propagating along certain latitudes (Fig. 6a, e and f). This behavior is likely to be connected to the ubiquitous eddy-driven generation of multiple alternating jets on PV gradients (e.g., Berloff et al. (2011)), if the eddy trains can rectify into the jets. Some other solutions develop pronounced beams of eddies radiating from the plunger at some angle (Fig. 6d), and many solutions combine several patterns. Pattern variations are large, because of the large variations of the underlying linear-mode dispersion properties: each flow solution consists of the Fourier normal modes, that have the same frequency $\omega_0$, and of the set of broadly distributed wavenumbers, that are selected by the shape of the forcing and by the dispersion relation. All these constraints result in the solution populated with specific sets of wavenumbers. The resulting phase relationships couple the involved Fourier harmonics with the imposed forcing and each other.

For the plunger-induced solutions we introduced the concept of *footprint*, which is the central aspect of the proposed parameterization. The footprint $P_i(x,y)$ is defined as the layer-wise time-mean nonlinear self-interaction of the linear plunger-induced solution, that is, as the divergence of the corresponding PV fluxes. Footprints quantify eddy feedback on the large-scale flow. Footprint can be projected on the barotropic and baroclinic modes, and its components are $P^{(brt)}$ and $P^{(bcl)}$, respectively. Footprints do not have meaningful amplitude, because of the problem linearity, but their

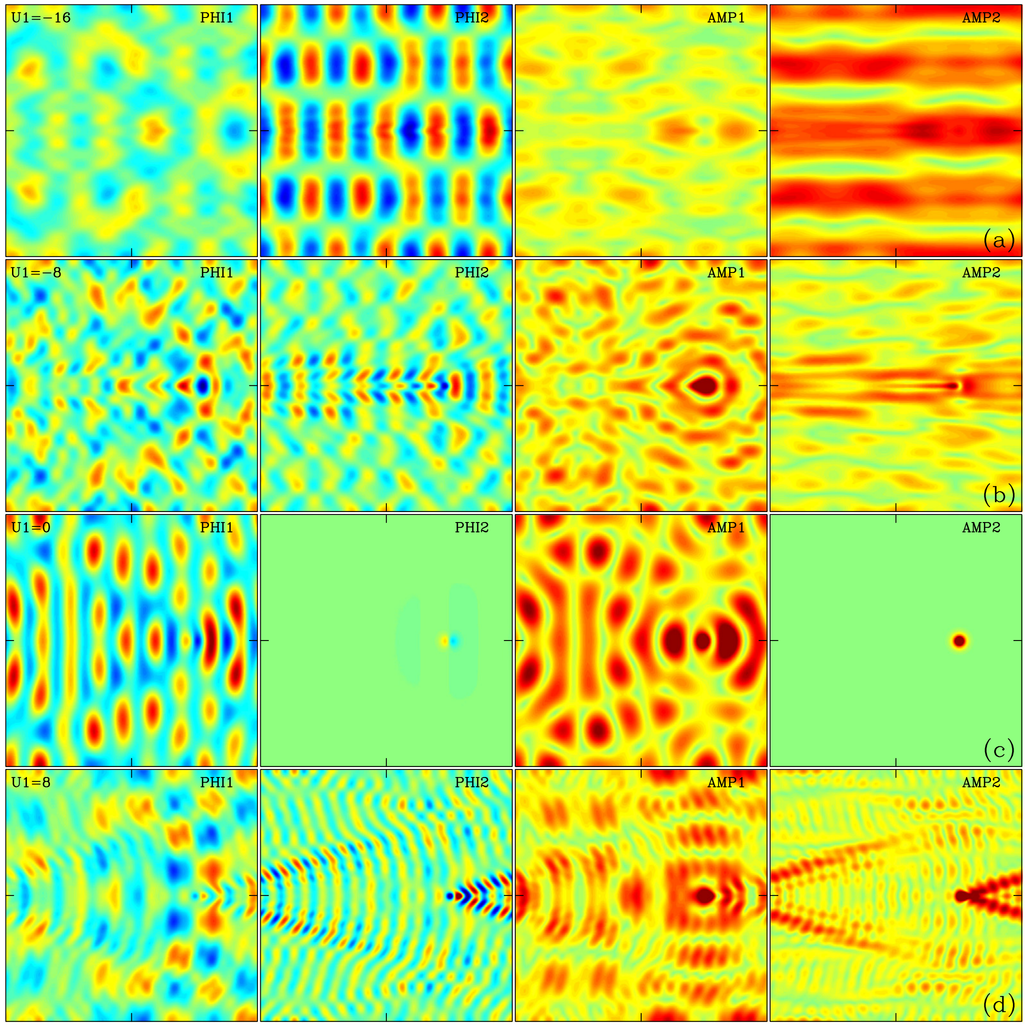


**Fig. 6.** Two-layer linear flow responses to the localized oscillating forcing (plunger). Individual solutions are shown in rows, and for $U_1$ equal to (a) −16, (b) −8, (c) 0, (d) 8, (e) 16, (f) 30, and (g) 45 cm s$^{-1}$ (with $U_2 = 0$). The plunger period is $T = 65$ days. The center of the plunger is located at $(x_0, y_0) = (0.25L, 0)$, and $-L < x < L$, $-L < y < L$, and the solutions are doubly periodic. The first and second columns of panels show snapshots of the solution represented in terms of the barotropic and baroclinic velocity streamfunctions, respectively; the third and fourth columns of panels show the complex amplitudes of the barotropic and baroclinic components of the solution. All solutions are energy-normalized, and the arbitrarily chosen units are the same for all panels.

patterns are well defined. We normalized different $P_i(x, y)$ by the plunger amplitude and compared them with each other (Fig. 7). In general footprints have complicated patterns that reflect complexities of the plunger-induced solutions, and this complexity tends to increase with amplitude of the background shear. The shear has strong effect on the footprints not only in terms of their structural properties, due to the discussed baroclinic delocalization, but also in terms of their amplitude and integral properties, as shown further below.

Now, by providing relevant context let us justify usefulness of some bulk properties of the footprints. The main nonlinear flow response to a beta-plane barotropic plunger is the rectified eastward jet at the forced latitudes and weaker return flows adjacent to it (Haidvogel and Rhines, 1983; Berloff et al., 2005; Waterman and Jayne, 2012). By time-stepping the nonlinear model, we found that the tendency to generate this pattern persists in the baroclinic situation with the background shear. This tendency can be also viewed as the double-gyre eddy backscatter mechanism that maintains the eastward jet extension and its adjacent recirculation zones (Berloff et al., 2005b). Since our main interest is about plunger-induced nearly zonal currents, we focused on *zonally averaged* footprints, denoted to as $\langle P_i \rangle (y)$. Typical $\langle P_i \rangle$ is dominated by either 2 or 4 lobes with alternating sign grouped around $y_0$ (Fig. 7). The larger lobes are located around $(x_0, y_0)$, and the smaller lobes are located further away. Since footprints are antisymmetric around the central latitude $y_0$, $\langle P_i \rangle$ is also antisymmetric. We characterized $\langle P_i \rangle$, as well as the corresponding $\langle P^{(brt)} \rangle$ and $\langle P^{(bcl)} \rangle$, by their integral values over the northern half of the domain. These values are referred to as *elementary footprints* and denoted as $E_i, E^{(brt)}$ and $E^{(bcl)}$. We found that for positive and weakly negative $U_1$ both $E^{(brt)}$ and $E^{(bcl)}$ are positive, implying that the footprint must induce a large-scale jet with both barotropic and baroclinic components being eastward. However, when $U_1$ is strongly negative, both $E^{(brt)}$ and $E^{(bcl)}$ are negative, implying the footprint westward barotropic and baroclinic jet components.

To demonstrate how the simple parameterization works, we focused on the upper-layer elementary footprint $E_1$ and on its dependencies on the background flow and other parameters of the problem, and considered wide range of background flows: $-20 < U_1 < 60$ cm s$^{-1}$. We found that when $|U_1|$ is small, $E_1$ is small and the plunger period $T$ has modest effect on the elementary footprint. On the contrary, for relatively large $|U_1|$, $E_1$ reaches maximum and is positively correlated with $T$ (Fig. 8). This implies that, in terms of the feedback on the large-scale flow, the transient

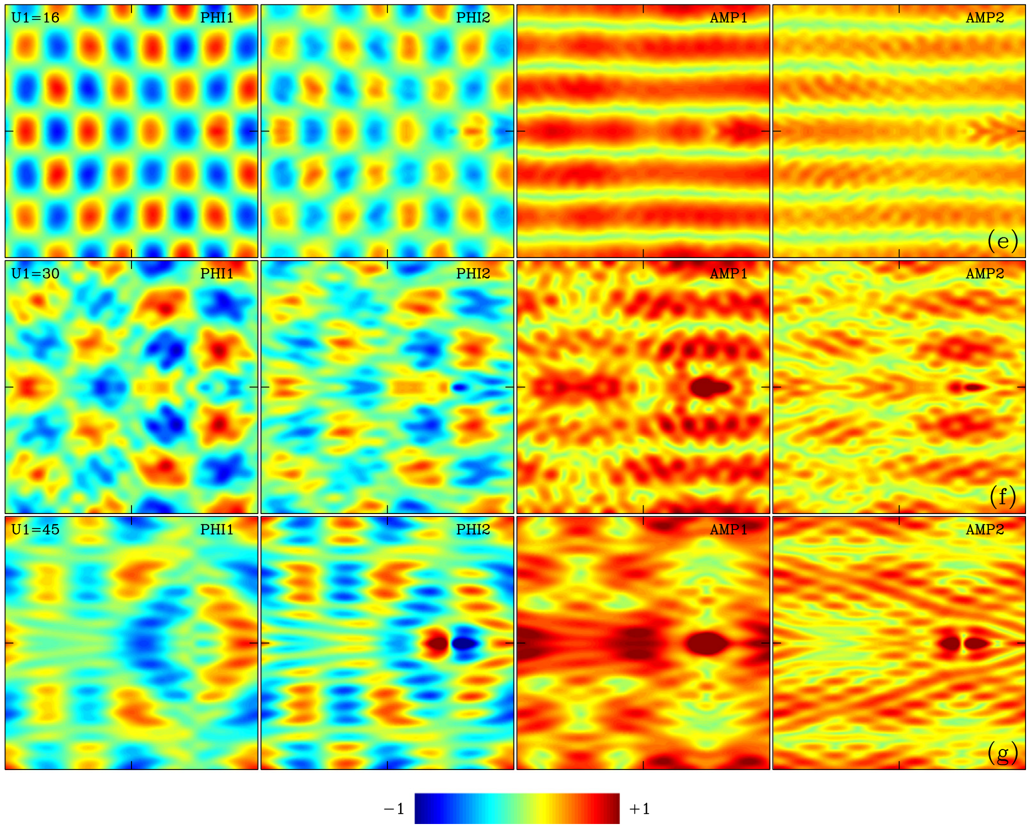


**Fig. 6** (*continued*)

eddy forcing must be the most efficient for moderate vertical shears and longer time scales.

If $U_1 < -5\ \mathrm{cm\,s^{-1}}$, then $E_1$ is negative, otherwise $E_1$ is positive; and for large $|U_1|$ the elementary footprint again becomes small. This implies that the plunger (or the actual transient eddy forcing) must induce an eastward jet, but when this jet becomes strong, the plunger effect must be weakened. This weakening can be interpreted as a bounding mechanism on the eddy-induced zonal jet. Long plunger periods result in larger $E_1$ and, therefore, must favor jet rectification, but the actual eddy forcing periods are constrained by the dynamics and limited to relatively narrow range of values (Section 2). In the double gyres, this range is probably constrained by the Rossby deformation radius $Rd_1$, which sets the eddy length scales and, thus, through the linear dispersion relation fixes the corresponding time scales. We can not easily vary $Rd_1$ in the double-gyres, because of the massive computational costs, but we varied $Rd_1$ in the plunger problem. We found that shorter $Rd_1$ noticeably reduces the elementary footprint, and more so for $U_1 < 0$. This suggests that the strongest effect of the eddy forcing must correspond to the first baroclinic mode, which has the longest baroclinic deformation radius, and the eddy forcing components acting on the higher baroclinic modes must play progressively weaker roles in the rectification. This conjecture is in the sharp contrast with the proposition that the higher baroclinic modes play a catalytic role for enhancing the eastward jet (Barnier et al., 1991), but more systematic studies beyond the scope of this paper are needed to resolve the disagreement. Also, larger $Rd_1$ makes the value of $U_1$ at which $E_1$ changes sign even more negative (Fig. 9), suggesting that the plunger is less efficient for inducing a westward jet, and even more so for higher baroclinic modes.

The only significant effect associated with plunger radius $r_0$ is its positive correlation with strength of the elementary footprints (Fig. 10). The infinitesimal $r_0$ corresponding to the $\delta$-function plunger, results in the infinitesimal footprint (see also Waterman and Jayne (2012)). We studied the dependence on the eddy viscosity $\nu$ by varying it from 10 to $200\ \mathrm{m^2\,s^{-1}}$ (Fig. 11) and found that $\nu$ is negatively correlated with the footprint strength, and this effect is more pronounced in the westward background shear. In general, the enhanced sensitivity of the westward shears to transient forcing is consistent with intensive generation of coherent vortices in the corresponding nonlinear large-*Re* flow regimes (Berloff et al., 2011), but more systematic research, beyond the scope of this paper, is needed to unravel the underlying physics.

We extended the above-described parameter dependencies to the three-layer dynamics, because it directly links the plunger studies to the double-gyre model and eddy parameterization. In the three-layer model, the vertical large-scale shear is constrained by (23), and the main dynamical difference from the two-layer case is due to the second baroclinic mode. We found that most aspects of the three-layer and two-layer plunger solutions are qualitatively similar, therefore, we discuss only the main differences. First, contrast between the footprints in the eastward and westward background shears is much weaker in the three-layer formulation (Figs. 12 and 13), mostly due to weaker footprints in the westward shear. Second, in the three-layer case the range of negative elementary footprints is narrower. All of this suggests that severe truncation of the vertical degrees of freedom may exaggerate the sensitivity of the westward shears to transient forcing.

To summarize, discussed in this section study of the plunger-induced solutions and their footprints provides us not only with the fundamental understanding of the transiently forced dynamics, but also with the essential relationships between the induced footprint and the background flow.

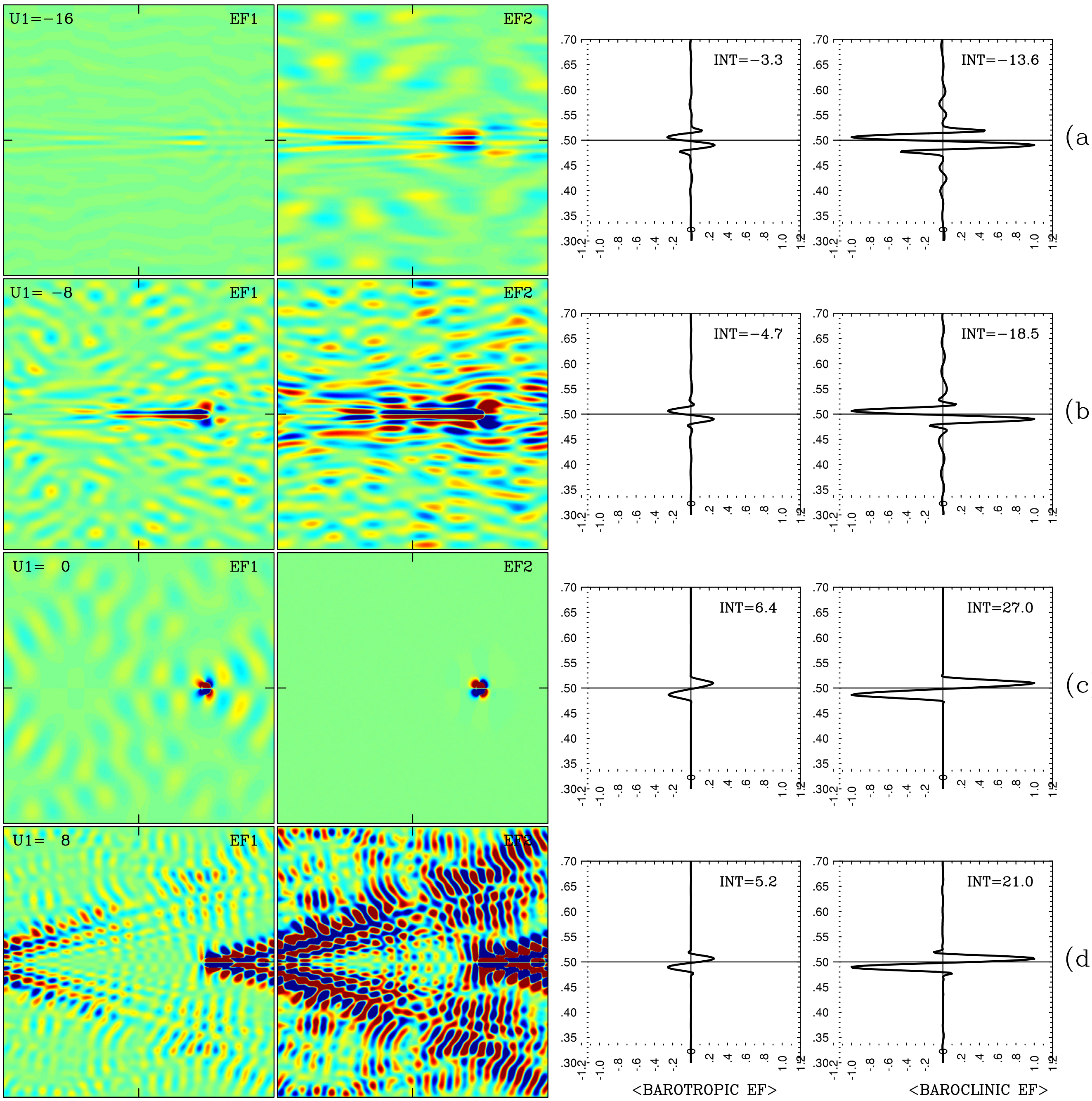


**Fig. 7.** Eddy forcing patterns (footprints) corresponding to the plunger-induced solutions from Fig. 6. Individual footprints are demonstrated in rows, and the rows correspond to $U_1$ equal to (a) −16, (b) −8, (c) 0, (d) 8, (e) 16, (f) 30, and (g) 45 cm s$^{-1}$. The first and second columns of panels show the barotropic and baroclinic footprint components, respectively. The footprints are obtained for the energy-normalized solutions, and the displayed units are arbitrary but the same over all panels. The third and fourth columns of panels show the profiles of the zonally averaged barotropic and baroclinic components of the corresponding footprint, respectively. The profile pairs are normalized so that their maximum absolute value is unity. The integral value of each profile is found over the northern half of the domain and indicated on each panel (with $10^{-3}$ units) — this is the elementary (barotropic or baroclinic) footprint.

## 5. Implementation and tests of the eddy parameterization

In the previous section, we established relation between the three-layer footprint and the background shear and stored this relation in terms of the functional dependence $E_1 = E_1(U_1)$, calculated for the integer values (in cm s$^{-1}$) of $U_1$ $U_2$ and $U_3$ are related to $U_1$ via (23) and linearly interpolated in between. Thus, in a non-eddy-resolving model $E_1(t,x,y)$ can be straightforwardly obtained from the explicitly resolved large-scale zonal velocity $u_1(t,x,y)$. Next, we introduce the concept of *elementary footprint dipole*, which is a dipole at $(x_0, y_0)$ consisting of the PV anomaly $E_1$ north from $(x_0, y_0)$, and PV anomaly $-E_1$, south from it. The distance between the dipole anomalies is taken as the distance between the maximum and minimum values of the corresponding zonally averaged footprint $\langle P_i \rangle$ (Fig. 7). From the footprint analyses we found that for the relevant parameters this distance is slightly less than 60 km, which is the radius of the imposed forcing function. Therefore, given that our non-eddy-resolving model (discussed below) has the nominal grid resolution of 30 km, we set the dipole length to 60 km (2 grid intervals).

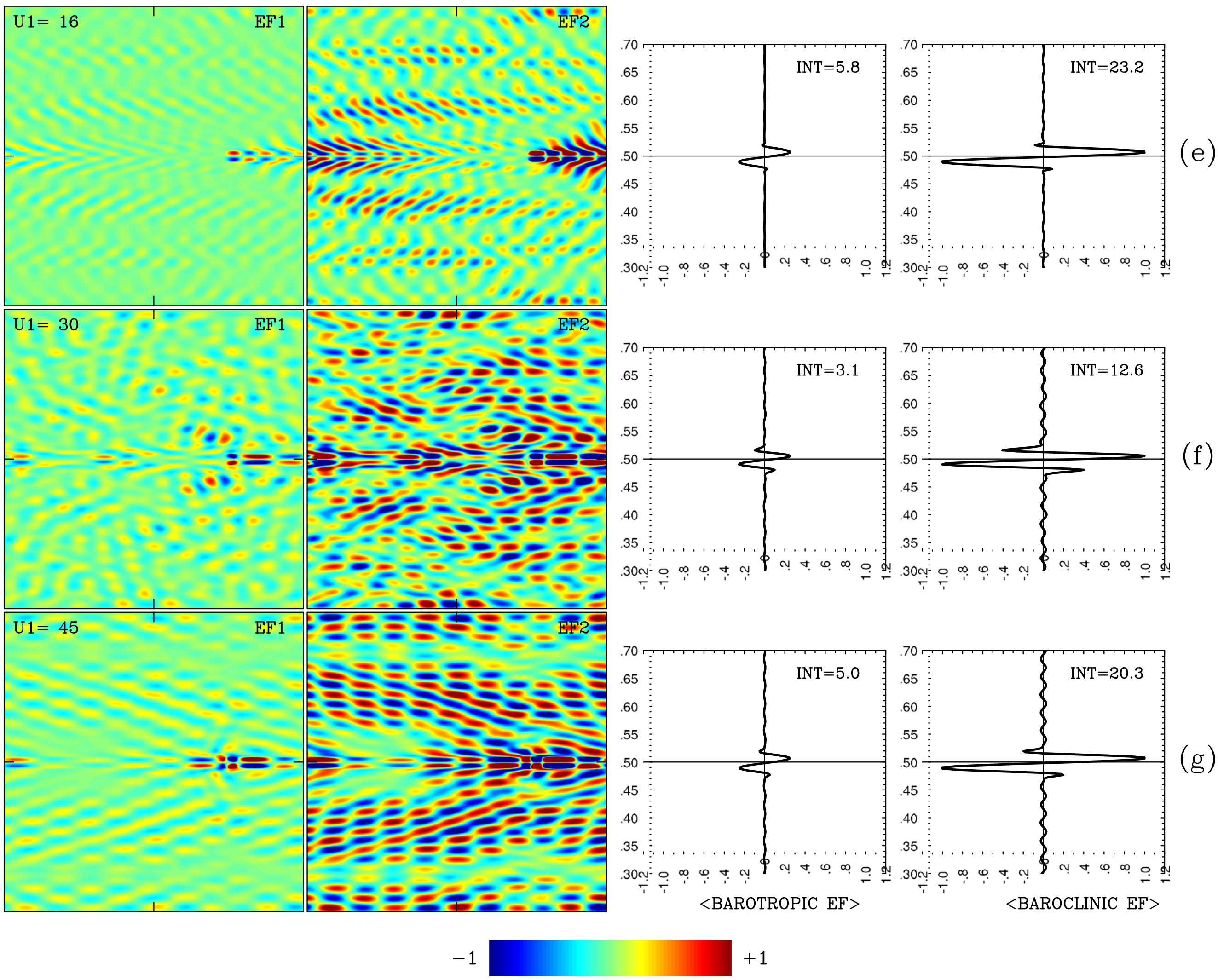


**Fig. 7** (*continued*)

The structure and strength of the elementary footprint dipole are defined by the linear dynamics, but its amplitude $D$ must be additionally defined by proper scaling and closed on the large-scale flow. Dimensional scaling of a footprint is that of the divergence of eddy PV fluxes, that is, eddy forcing. Hence, we assume that amplitude of the plunger forcing, which imitates the actual transient eddy forcing, is proportional to the magnitude of large-scale PV flux divided by some characteristic length scale. The latter is taken proportional to the spatial correlation length scale $r_0$ diagnosed from the double-gyres, so that:

$$D = C\frac{|\overline{\mathbf{u}}_1\overline{\mathbf{q}}_1|}{r_0}, \tag{45}$$

where $\overline{u_1}$ and $\overline{q_1}$ are the upper-layer large-scale velocity and PV anomaly, respectively, and, thus, the denominator is explicitly resolved by the non-eddy-resolving model. In the following analyses we assume that the nondimensional proportionality coefficient $C$ is unity. This leaves potential for further refinements, which are beyond the scope of this paper. The flux in (45) must eventually come from the non-eddy-resolving model, but its amplitude and pattern must be similar to those from the benchmark reference solution. The corresponding reference time-mean PV fluxes are shown in Fig. 14 illustrating that the upper-ocean flux, which is concentrated in the western boundary currents and their eastward jet extension, dominates over the deep-ocean flux by the order of magnitude. Another relevant observation is that the maximum flux values are shifted to the northern flank of the eastward jet.

We implemented the parameterization only in the eastward jet region denoted by rectangle in Fig. 14a, because this is the region with the most important eddy effects and flow rectification (Berloff et al., 2005a,b), and the simple parameterization is so far based only on the zonal component of the background flow that clearly dominates the region. The parameterized cumulative eddy forcing is given by adding up elementary footprint dipoles calculated at every grid point around the eastward jet and scaled by (45). The corresponding field calculated for the reference time-mean solution is shown in Fig. 15. It consists of the narrow positive and negative strips surrounding the eastward jet in a such way, that they have to maintain it.

Now, let us focus on formulating a coarse, non-eddy-resolving model of the double gyres. This model is exactly the same as the reference eddy-resolving model, except that it is solved on much coarser grid, with 30 km nominal resolution, and it has large eddy viscosity $\nu = 600\ \mathrm{m^2\ s^{-1}}$, so that the flow solutions are numerically converged and spatially smooth. The straightforward non-eddy-resolving solution (Fig. 16) differs dramatically from the eddy-resolving one, because it has no eastward jet. The kinetic energy

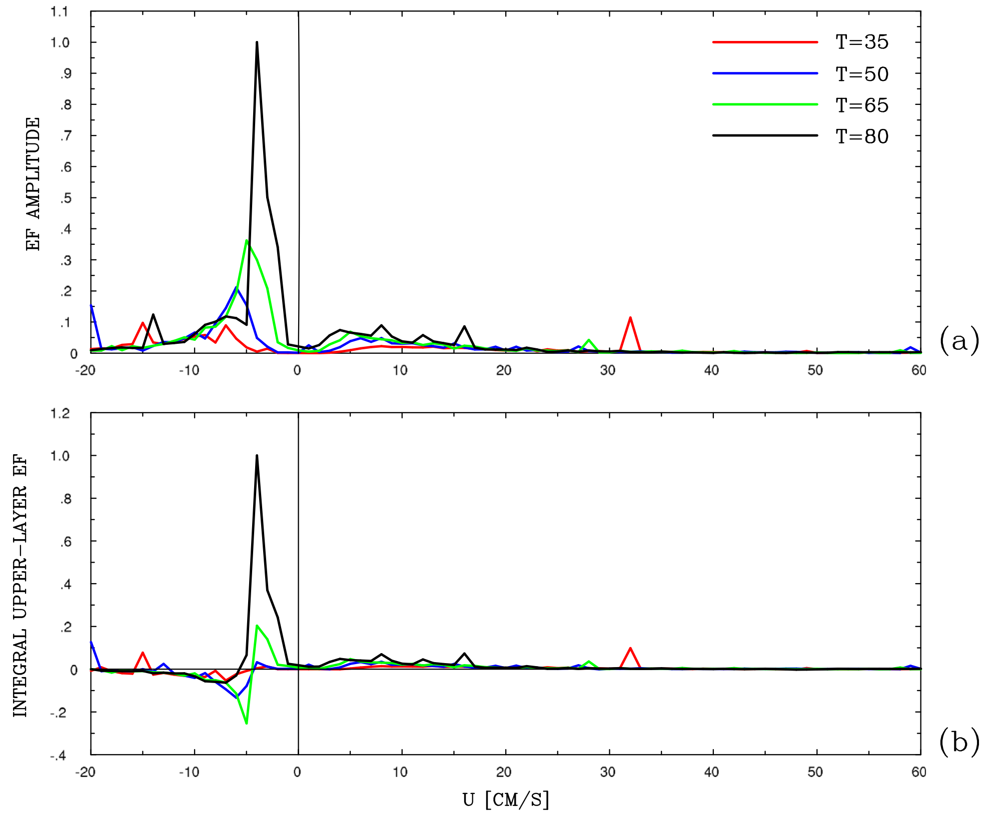


**Fig. 8.** Dependence of the two-layer footprint (eddy forcing) properties on the plunger period, *T*. The horizontal axis corresponds to the background velocity, $U_1$, and the vertical axis indicates (a) the maximum absolute value of the upper-layer zonally averaged footprint, and (b) the corresponding elementary footprint. All solutions are energy-normalized, and the units are arbitrary. Plunger periods $T = 35$, 50, 65 and 80 days are indicated by different colors. Note well-pronounced minimum around $U_1 = 0$.

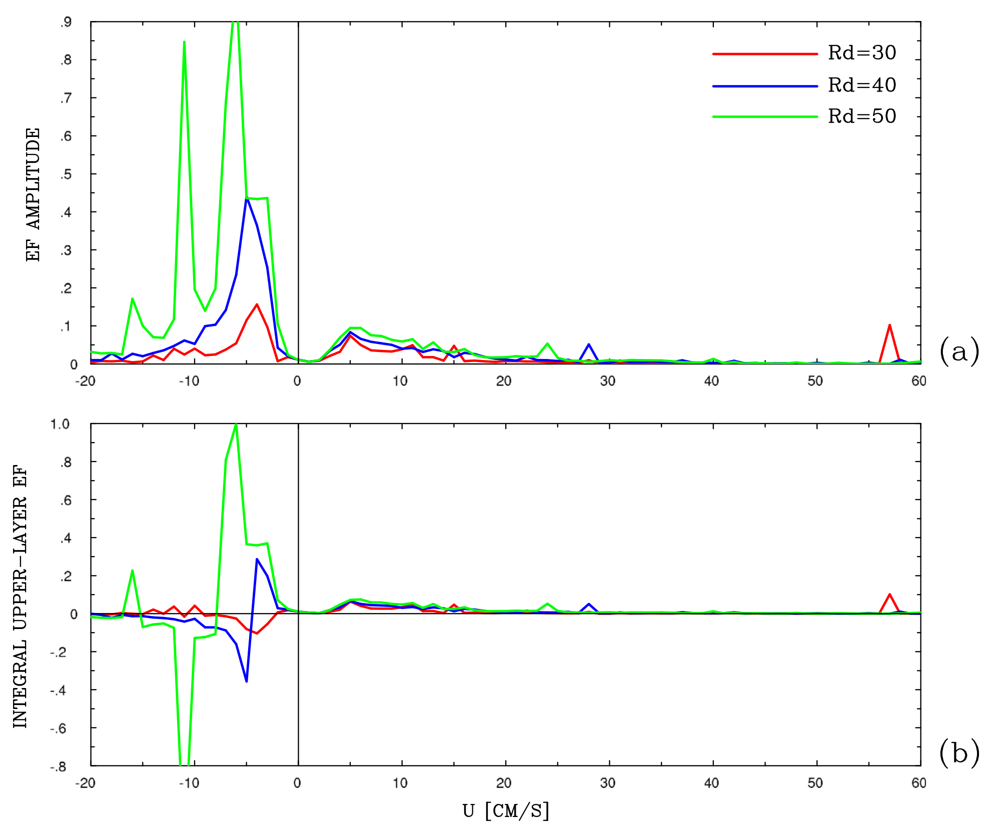


**Fig. 9.** Dependence of the two-layer footprint (eddy forcing) properties on the Rossby deformation radius, *Rd*. The outline is the same as in Fig. 8. The dependencies are shown for $Rd = 30$, 40 and 50 km (different colors). Note that for larger *Rd* the transition from positive to negative elementary footprints shifts to more negative $U_1$.

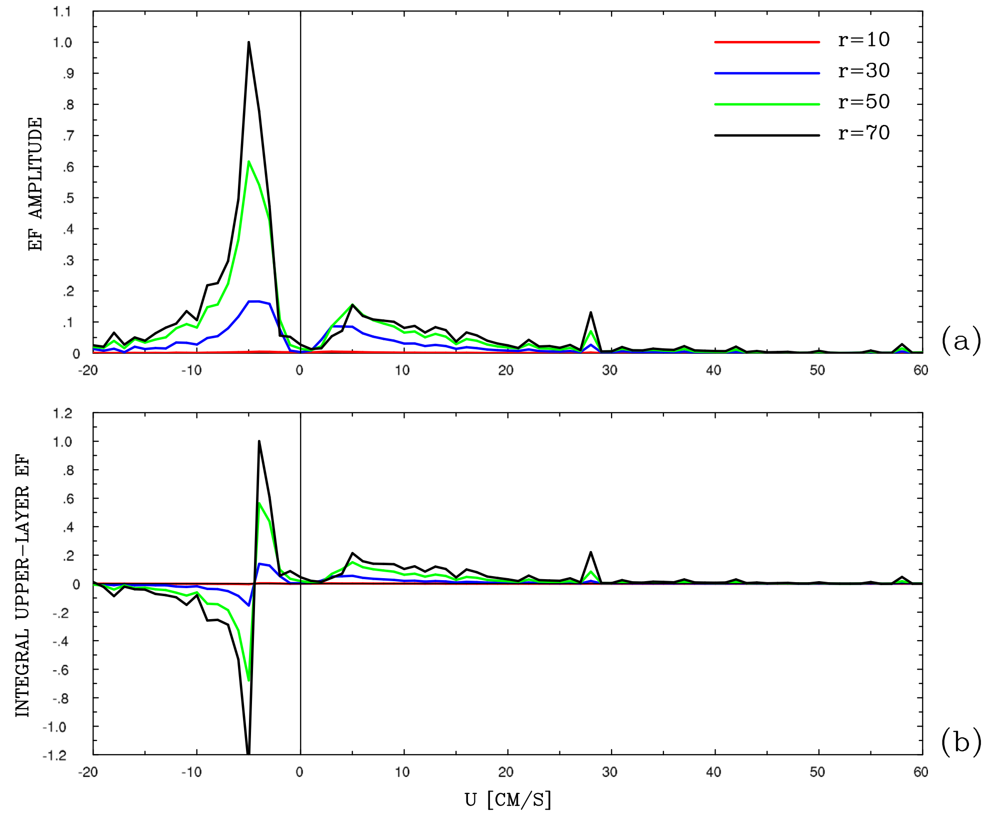


**Fig. 10.** Dependence of the two-layer footprint (eddy forcing) properties on the plunger radius, $r_0$. The outline is the same as in Fig. 8. The dependencies are shown for $r_0 = 10$, 30, 50 and 70 km (different colors). Note that the eddy forcing nearly vanishes for the smallest $r_0$.

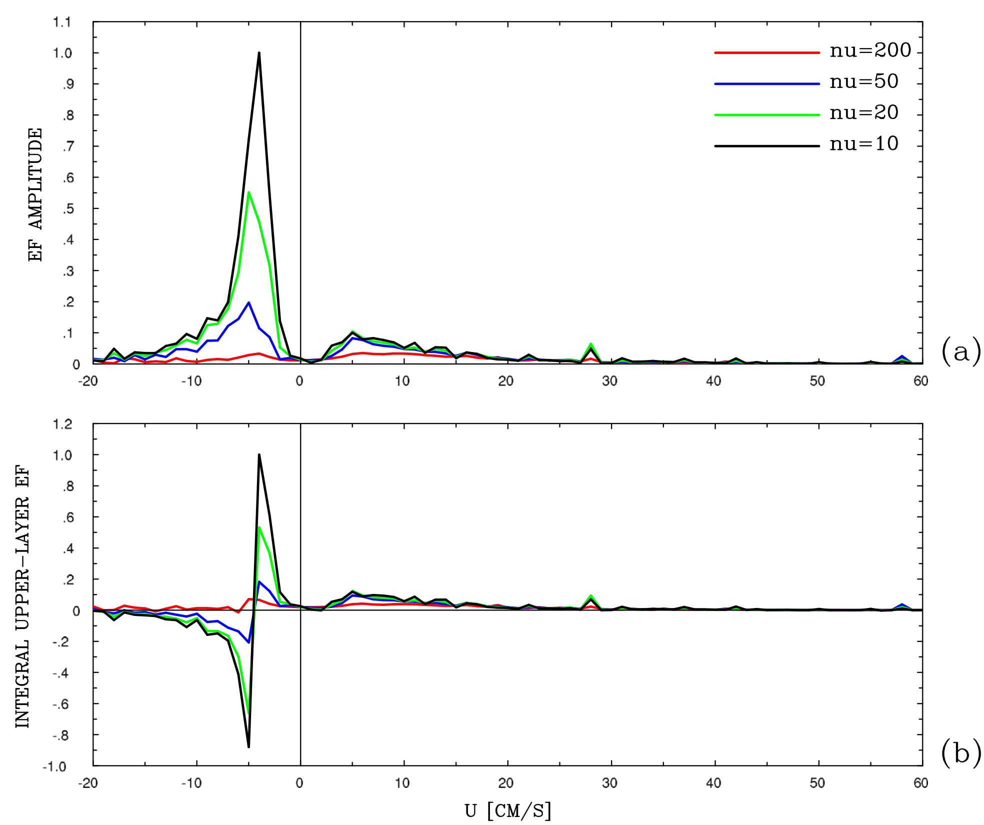


**Fig. 11.** Dependence of the two-layer footprint (eddy forcing) properties on the eddy viscosity, $\nu$. The outline is the same as in Fig. 8. The dependencies are shown for $\nu = 200$, 50, 20 and 10 $m^2\,s^{-1}$. Note the amplification of the eddy forcing for negative $U_1$.

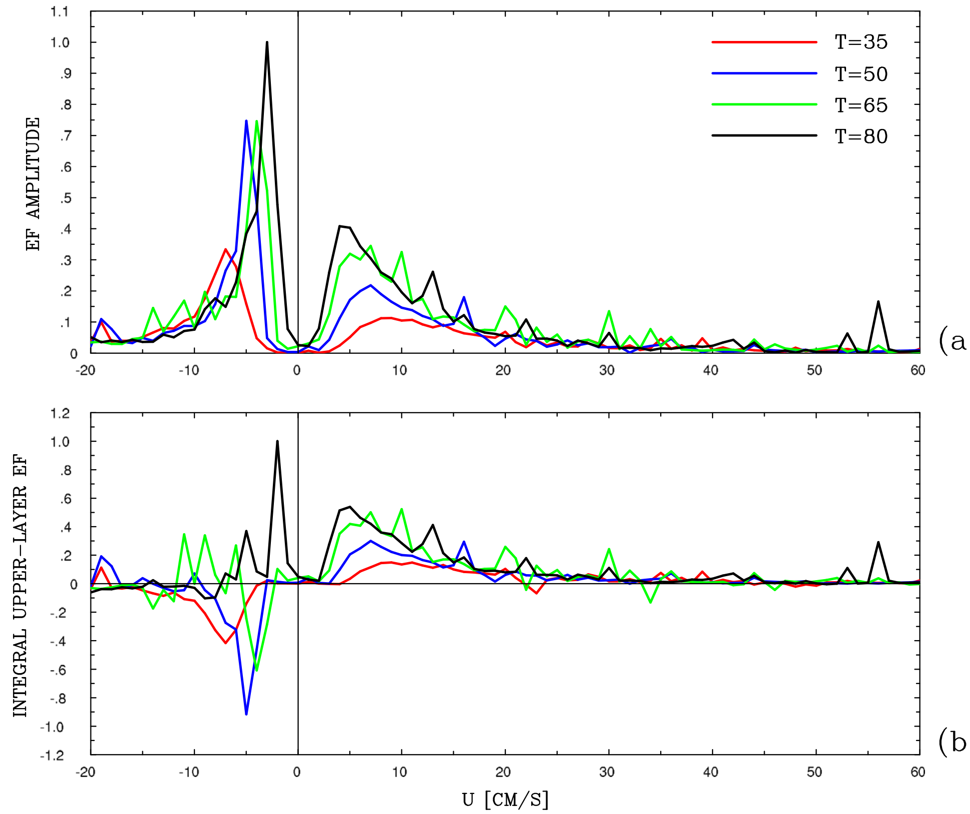


**Fig. 12.** Dependence of the three-layer footprint (eddy forcing) properties on the plunger period, *T*. The outline is the same as in Fig. 8, and shown are the upper-layer properties. The middle- and deep-layer background flow velocities are given by (23). Note the reduced contrast between the footprints in the eastward and westward background flows.

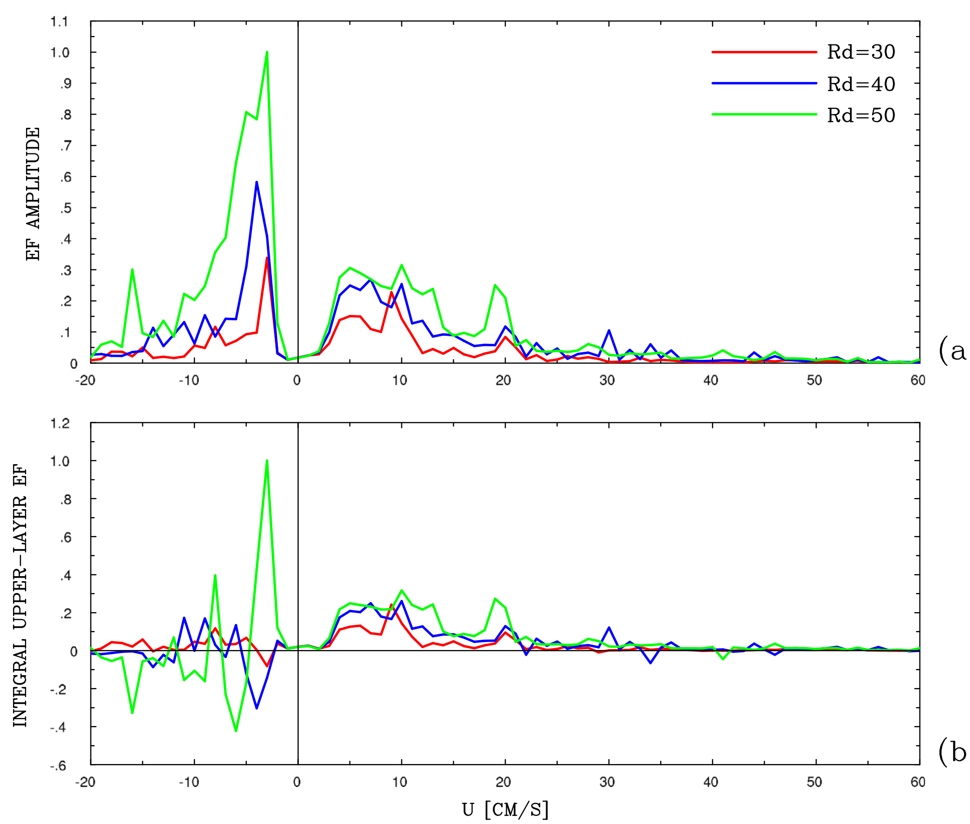


**Fig. 13.** Dependence of the three-layer footprint (eddy forcing) properties on the first Rossby deformation radius, *Rd*. The outline is the same as in Fig. 12.

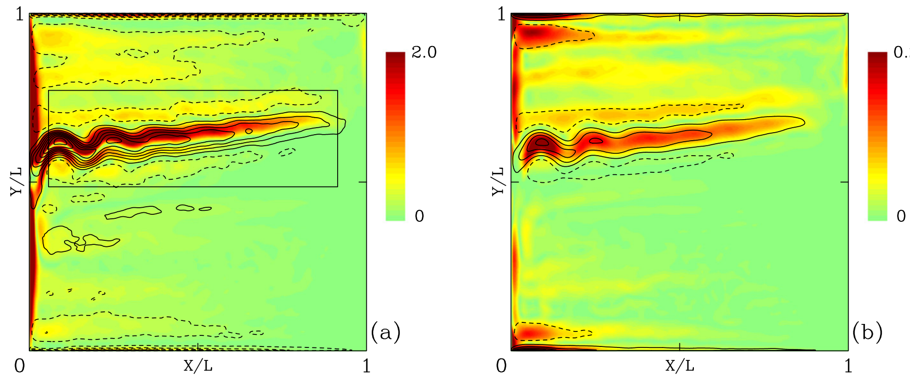


**Fig. 14.** Potential vorticity flux of the time-mean eddy-resolving reference solution. Shown are the absolute values of the flux in the (a) upper and (b) middle isopycnal layers (color; units are $10^{-5}$ m s$^{-2}$), superimposed on the corresponding time-mean zonal velocity component (contours; CI = $10^{-2}$ m s$^{-1}$). Rectangle on the left panel indicates the region of predominantly zonal time-mean flow and the most intensive eddy backscatter — this is the region where the eddy parameterization is implemented.

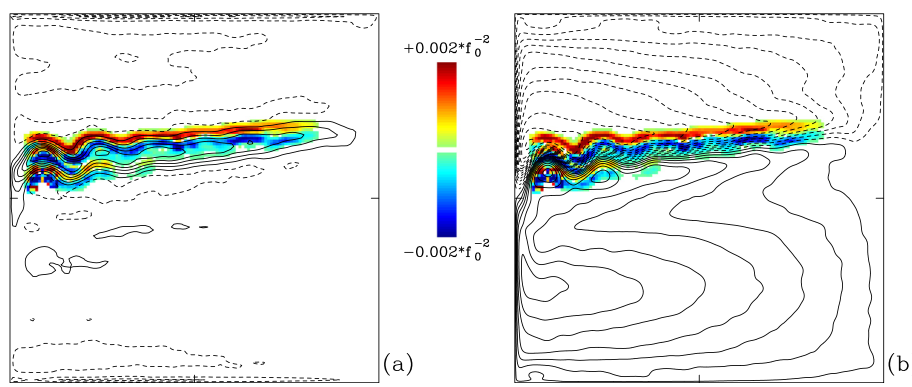


**Fig. 15.** Parameterized upper-ocean eddy forcing (color) estimated from the plunger dynamics on the basis of the reference time-mean circulation. The eddy forcing field is superimposed on the reference time-mean (a) zonal velocity component (CI = $10^{-2}$ m s$^{-1}$) and (b) transport streamfunction (CI = 2 Sv).

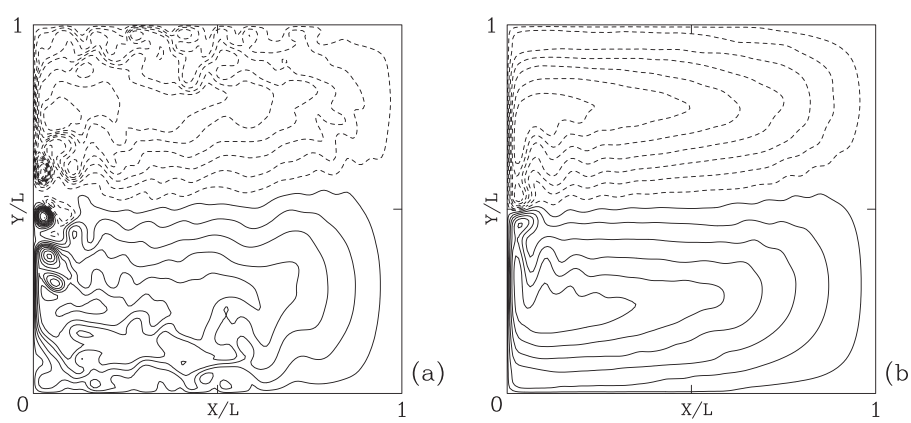


**Fig. 16.** Failure of the non-eddy-resolving model to simulate the eastward jet and its adjacent recirculation zones without a parameterization representing the eddy backscatter. Shown are the upper-ocean transport streamfunctions: (a) instantaneous and (b) the time-mean (CI = 2 Sv).

of the upper-ocean time-mean flow in the quarter of the basin that should contain the jet ($0 < y < L/2$) is only 19% of its reference value. Varying $\nu$ does not help to resolve the eastward-jet problem, because the eddy dynamics is profoundly misrepresented in the coarse model. A good eddy parameterization added to the coarse model must be able to fix the jet problem by accounting for the missing eddy forcing.

First, we tested the eddy parameterization in the unclosed form. For this purpose we imposed the cumulative eddy forcing pattern parameterized on the basis of the benchmark time-mean circulation and shown in Fig. 15. Implementation of the unclosed parameterization results in dramatic improvement of the coarse model in terms of the recovered eastward jet and its adjacent recirculation zones (Fig. 17). Not only the jet is robustly present in the coarse solution, but also the main resolved eddy activity is shifted from the western boundary currents to the region surrounding the jet, as in the reference solution. The kinetic energy of the upper-ocean time-mean flow in the quarter of the basin that should contain the

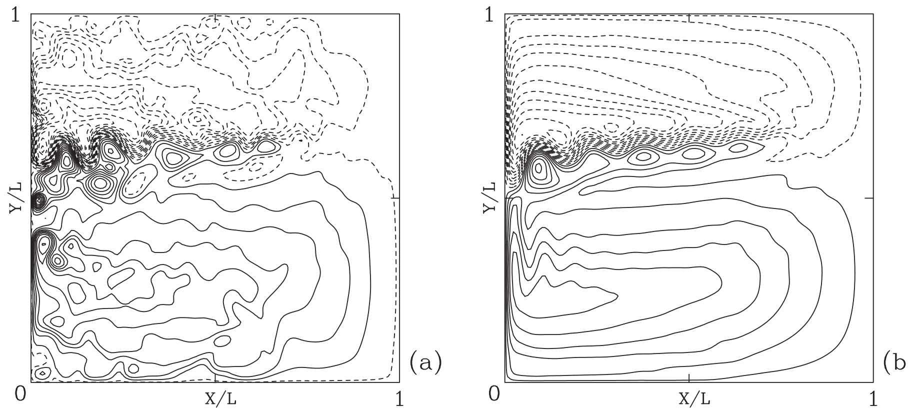


**Fig. 17.** Outcome of the unclosed parameterization added to the non-eddy-resolving model. The outline is the same as in Fig. 16. Note that this solution has well-developed eastward jet and its adjacent recirculation zones. The parameterization consists of the eddy forcing calculated from the time-mean standard flow and shown in Fig. 15; the involved parameters do not evolve with the large-scale flow, thus, keeping the parameterization unclosed.

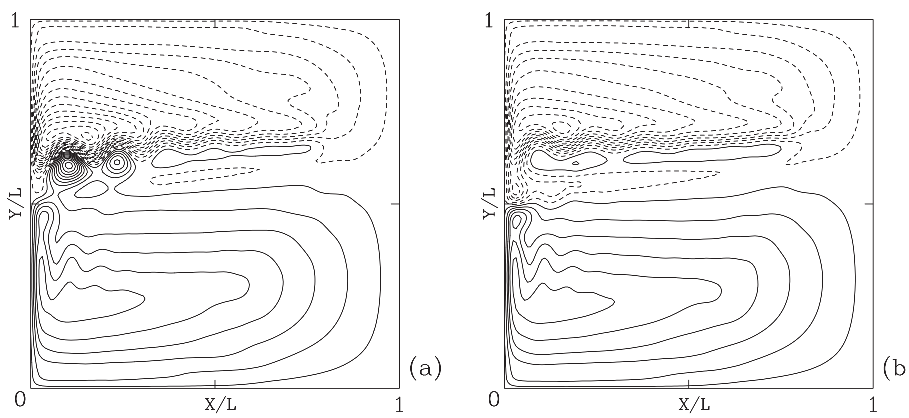


**Fig. 18.** Outcome of the fully closed parameterization added to the non-eddy-resolving model. (a) Time-mean upper-ocean transport streamfunction (CI = 2 Sv) for the reference case discussed in the text. Note that the eastward jet is close to the standard one shown in Fig. 4a, and there is massive improvement of the non-eddy-resolving and nonparameterized solution shown in Fig. 16. (b) Sensitivity study: the same as (a) but with the parameterized eddy forcing amplitude reduced by 10%.

jet $(0 < y < L/2)$ is now 82% of its reference value. The unclosed parameterization exercise proved that our parameterization is remarkably accurate, given the basic simplifications and interim short cuts of the algorithm.

Finally, we tested the eddy parameterization in its closed form by relating its parameters to the dynamically evolving large-scale flow. The unclosed parameterization results (Fig. 17a) told us that even in the coarse model the resolved eddy activity is significant, therefore, relating the parameterization to the instantaneous flow is fraught with double counting the eddy effects. In practice this results in locally large transient westward shear that induces overly strong footprints; the resulting PV anomalies become accumulated into exaggerated recirculation zones around the eastward jet. To overcome this problem, we smoothed the coarse-model solution by the interactive running-average filter spanning the last 5 years of the solution. We varied the filter width and found that the outcome is not sensitive to it, as long as this width is interannual or longer, so that the resolved eddies are smoothed out. The fully parameterized model was spun up for 20 years and, then, solved for another 50 years. The solution is similar to the unclosed parameterized one, but the eastward jet is stronger in the western quarter of the basin and weaker in the middle of the basin (Fig. 18a). The kinetic energy of the upper-ocean time-mean flow in the quarter of the basin that should contain the jet $(0 < y < L/2)$ is remains at 82% of its reference value, as in the unclosed case. Overall, implementation of the closed parameterization results in dramatic improvement of the coarse model. To check robustness of the outcome, we studied its sensitivity to the proportionality coefficient $C$ in (45) and found that varying $C$ by 10% yields some quantitative changes but does not destroy the eastward jet (Fig. 18b).

To summarize, despite some interim simplifications, the proposed eddy parameterization significantly improves the non-eddy-resolving model. We developed the parameterization algorithm, understood its dynamical underpinnings, and demonstrated that it works in practice. Some further improvements are discussed in the next section.

## 6. Summary and discussions

This paper aims at developing a framework for dynamically consistent parameterization of the oceanic, mesoscale (geostrophic) eddy effects for use in non-eddy-resolving ocean circulation models. Here, the *parameterization* is a simple, parametric mathematical model that accounts for the unresolved but important eddy fluxes which affect the large-scale circulation. A failure to account for the eddy effects typically results in gross errors in the simulated ocean circulation that have many negative consequences. The *dynamical consistency* means that the parameterization invokes explicit solutions of a simplified dynamical problem, rather than ad hoc assumptions. The *framework* means that we provide the guiding idea and principles for developing the parameterization algorithm, rather than the refined final result.

The brute-force alternative to eddy parameterization is to resolve the eddies dynamically, but, due to the required enormous computational costs, this will remain practically unfeasible for long time, providing high demand for accurate and efficient eddy parameterizations. The most common parameterization of the eddies is the isopycnal or horizontal eddy diffusion of buoyancy and momentum, that is routinely implemented in non-eddy-resolving oceanic components of global climate models. The main problem of the eddy diffusion is that it is fundamentally wrong in the common (but not prevailing) "negative diffusivity" situations characterized by anti-diffusive (i.e., up-gradient) eddy fluxes. The other common problem is that, eventually, any parameterization must be *closed* in the sense that its parameters (e.g., eddy diffusivity) are to be obtained from the properties of the explicitly resolved large-scale circulation. Closing a parameterization is usually more difficult than formulating its mathematical algorithm.

In order to put forward and test the proposed parameterization framework, we focused on the classical, wind-driven double-gyre model, and studied its reference solution, as well as the corresponding divergence of the eddy potential vorticity (PV) fluxes. This divergence can be interpreted as the eddy forcing exerted on the large-scale flow. We focused on the transient rather than time-mean component of the eddy forcing, because in the gyres it is responsible for the dominant eddy effect (Berloff et al., 2005b). This effect, also known as eddy backscatter, is the eddy-induced generation of the eastward jet extension of the western boundary currents. Since this eddy effect is associated with up-gradient eddy fluxes, it is notoriously difficult to parameterize diffusively. Therefore, some recent efforts made towards its parameterization discard the diffusion and try to represent the eddy effects in terms of transient (random) forcing. Precursors of the present work are Berloff et al. (2005a,b) and Porta Mana and Zanna (2014), where the transient eddy forcing is modeled as a random, space–time correlated forcing added to the non-eddy-resolving dynamics. The capability to represent the eddy backscatter is the main advantage of this approach, and we took it several steps further. The novelty is the use of flow responses to the elementary transient forcings as the building blocks of the parameterization, and relation of these responses to the large-scale flow properties.

First, we analyzed the reference eddy-resolving solution, estimated the characteristic length and time scales of the transient eddy forcing and used them to construct the transient forcings, referred to as the plungers. We also obtained the reference time-mean circulation and used it later as the benchmark for assessing the parameterization skills. Second, we systematically studied the linear-dynamics plunger solutions and their dependencies on the underlying large-scale flow and other physical parameters. These solutions can be viewed as the convolutions of the Green's functions of the problem. For each solution we found its nonlinear self-interaction, referred to as the *footprint* of the plunger. We found that each footprint strongly depends on the underlying large-scale flow, and, thus, provides us with the closure relationship. Since footprints come from the linear dynamics, their amplitude has to be scaled properly, and we scaled it with the large-scale PV fluxes and correlation length scale. Third, we implemented the parameterization in the non-eddy-resolving double-gyre model and verified that it works, in the sense that it facilitates development of the eastward jet and its adjacent recirculation zones and, thus, results in the massive improvement of the model.

The parameterization algorithm consists of the following steps. The first step is collection of the relevant large-scale flow fields from the non-eddy-resolving model. These fields are so far represented by the upper-ocean distributions of the zonal velocity and magnitude of the PV flux. The second step is converting the large-scale flow information into the ensemble of local footprints, that are added up to provide the cumulative eddy forcing correction to be imposed on the model. This step explicitly involves solving the linearized dynamics that transforms localized transient forcing into the corresponding footprint. The linearized-dynamics problem is solved only once and for all times, and the parameterization only refers to the precomputed information. Because of the explicit use of the dynamics, the parameterization is referred to as *dynamically consistent*. The third step is the time stepping of the non-eddy-resolving model; then, the first step is repeated.

Let us now discuss some connections between our study and some recent works. First, our extended Green's function approach to the problem is complimentary to the approach that estimates eddy diffusivities from the local linear-stability analysis (e.g., Eden (2011)). Both approaches utilize the linear dynamics, but here we do not rely on the most unstable linear normal modes. Second, an interesting parallel can be drawn with Srinivasan and Young (2014), where the Reynolds stress is found for randomly forced, $\beta$-plane barotropic dynamics linearized around uniform horizontal shear. Depending on the degree of anisotropy of the spatially homogeneous and correlated, white-noise forcing, and on the background shear, the Reynolds stress can induce either positive or negative eddy viscosity effect. Similar, or study relies on the transformation of external forcing by the linear dynamics and on the use of the outcome to find the nonlinear stress (i.e., eddy forcing), but several other aspects make it quite different: first, we considered spatially inhomogeneous and temporally periodic external forcing; second, we studied multilayer baroclinic model with richer dynamics; third, we extended the results toward fully closed and successfully tested parameterization of the eddy effects in non-eddy-resolving ocean circulation model.

The proposed parameterization framework raises a number of interesting questions beyond the scope of this paper. Let us discuss briefly some conspicuous research avenues that are likely to yield significant improvements and refinements of the present parameterization. First, in the analysis of the footprints, we studied simple background flow effects due to horizontally uniform zonal currents. This simplification can be systematically upgraded toward realistic, inhomogeneous background flows; for example, by starting with meridionally localized zonal jets and moving, eventually, to realistic ocean gyres. Also, we used simple empirical relation between the background zonal velocities at different depths, but this relation can be straightforwardly relaxed, at the expense of some technical complexity. Second, we worked with relatively simple quasigeostrophic dynamics that combines the eddy momentum and buoyancy fluxes into the eddy PV flux, but this dynamical core can be upgraded, first, to the shallow-water model with stacked isopycnal layers, and, eventually, to the continuous primitive equations. Third, we considered temporally periodic plungers, but this assumption can be overhauled by considering more realistic and complicated models of the time evolution (e.g., random processes with built-in temporal correlations or short-time pulses). Fourth, we considered simple horizontal and vertical structure of the plungers, but these assumptions can be systematically overhauled by considering more realistic and less confined forcing functions, as well as their dependencies on the large-scale PV gradients. Fifth, a more detailed mathematical analysis of the plunger-driven linear solutions is left for the future. Such solutions were rarely studied in the past (e.g., Haidvogel and Rhines (1983), Waterman and Jayne (2012)), because of the dominance of the normal-mode and linear-stability approaches. Sixth, it is tempting to extend our study kinematically and to analyze plunger-induced eddy diffusivities, as well as other transport and mixing properties. Seventh, conceptual similarities and differences between our approach and the recent parameterization framework suggested by Grooms et al. (2015) ask for thorough evaluation. Finally, we obtained only *linear* plunger-driven solutions and, then, analyzed their nonlinear self-interactions, but future systematic analyses of the fully nonlinear plungers are anticipated.

## Acknowledgments

This work was largely inspired by the atmosphere of Woods Hole and its celebrated oceanographic community, as well as by discussions with Joe Pedlosky. Fruitful discussions with Arseni Goussev are also gratefully acknowledged. Part of this work was carried out in the Department of Applied Mathematics and Theoretical Physics, and its hospitality is acknowledged with gratitude.

## Appendix A. Three-layer plunger dynamics

The three-layer extension of the plunger-driven dynamics is explicitly compatible with the three-layer double-gyre model. Assuming that the forcing function is distributed over all layers, the system of equations is obtained similar to (36), (37):

$$-i(kU_1+\omega_0)\Big(-(k^2+l^2+S_1)\tilde{g}_1+S_1\tilde{g}_2\Big)-i\,\beta_1 k\,\tilde{g}_1-\nu(k^2+l^2)^2\tilde{g}_1=f_1, \tag{A1}$$

$$\begin{aligned}&-i(kU_2+\omega_0)\Big(-(k^2+l^2+S_{21}+S_{22})\tilde{g}_2+S_{21}\tilde{g}_1+S_{22}\tilde{g}_3\Big)\\&\quad-i\beta_2 k\tilde{g}_2-\nu(k^2+l^2)^2\tilde{g}_2=f_2,\end{aligned} \tag{A2}$$

$$-i(kU_3+\omega_0)\Big(-(k^2+l^2+S_3)\tilde{g}_3+S_3\tilde{g}_2\Big)-i\beta_3 k\tilde{g}_3-\nu(k^2+l^2)^2\tilde{g}_3=f_3, \tag{A3}$$

where

$$\begin{aligned}&\beta_1=\beta+S_1(U_1-U_2),\quad \beta_2=\beta+S_{21}(U_2-U_1)+S_{22}(U_2-U_3),\\&\beta_3=\beta+S_3(U_3-U_2)\end{aligned} \tag{A4}$$

are the isopycnal background PV gradients, and the eddy viscosity term is added to the dynamics, as in the double-gyre model (the bottom friction term is absent, because we found its effect to be weak). Eqs. (A1)–(A3) can be written as

$$\mathbf{A}\begin{pmatrix}\tilde{g}_1\\ \tilde{g}_2\\ \tilde{g}_3\end{pmatrix}\equiv\begin{pmatrix}a & b & c\\ d & e & f\\ g & h & j\end{pmatrix}\begin{pmatrix}\tilde{g}_1\\ \tilde{g}_2\\ \tilde{g}_3\end{pmatrix}=\begin{pmatrix}if_1\\ if_2\\ if_3\end{pmatrix}, \tag{A5}$$

where the elements of matrix $\mathbf{A}$ are:

$$a=\beta_1 k-(kU_1+\omega_0)(k^2+l^2+S_1)-i\nu(k^2+l^2)^2, \tag{A6}$$

$$b=S_1(kU_1+\omega_0), \tag{A7}$$

$$d=S_{21}(kU_2+\omega_0), \tag{A8}$$

$$e=\beta_2 k-(kU_2+\omega_0)(k^2+l^2+S_{21}+S_{22})-i\nu(k^2+l^2)^2, \tag{A9}$$

$$f=S_{22}(kU_2+\omega_0), \tag{A10}$$

$$h=S_3(kU_3+\omega_0), \tag{A11}$$

$$j=\beta_3 k-(kU_3+\omega_0)(k^2+l^2+S_3)-i\nu(k^2+l^2)^2 \tag{A12}$$

and $c=g=0$. For each pair of wavenumbers $(k,l)$ the solution is given by Cramer's rule:

$$\tilde{g}_1=i\,\frac{(ej-fh)f_1+(ch-bj)f_2+(bf-ec)f_3}{\det(\mathbf{A})}, \tag{A13}$$

$$\tilde{g}_2=-i\,\frac{(dj-fg)f_1+(cg-aj)f_2+(af-cd)f_3}{\det(\mathbf{A})}, \tag{A14}$$

$$\tilde{g}_3=i\,\frac{(dh-eg)f_1+(bg-ah)f_2+(ae-bd)f_3}{\det(\mathbf{A})}, \tag{A15}$$

where $\det(\mathbf{A})=a(ej-fh)-b(dj-fg)+c(dh-eg)$.

## References

Barnier, B., Hua, B.L., Le Provost, C., 1991. On the catalytic role of high baroclinic modes in eddy-driven large-scale circulations. J. Phys. Oceanogr. 21, 976–997.
Berloff, P., 2005. On rectification of randomly forced flows. J. Mar. Res. 31, 497–527.
Berloff, P., 2005a. Random-forcing model of the mesoscale oceanic eddies. J. Fluid Mech. 529, 71–95.
Berloff, P., 2005b. On dynamically consistent eddy fluxes. Dyn. Atmos. Oceans 38, 123–146.
Berloff, P., McWilliams, J., 2003. Material transport in oceanic gyres. Part III: randomized stochastic models. J. Phys. Oceanogr. 33, 1416–1445.
Berloff, P., Kravtsov, S., Dewar, W., McWilliams, J., 2007. Ocean eddy dynamics in a coupled ocean–atmosphere model. J. Phys. Oceanogr. 37, 1103–1121.
Berloff, P., Karabasov, S., Farrar, J., Kamenkovich, I., 2011. On latency of multiple zonal jets in the oceans. J. Fluid Mech. 686, 534–567.
Dritschel, D., McIntyre, M., 2008. Multiple jets as PV staircases: the Phillips effect and the resilience of eddy-transport barriers. J. Atmos. Sci. 65, 855–874.
Eden, C., 2011. A closure for meso-scale eddy fluxes based on linear instability theory. Ocean Modell. 39, 362–369.
Gent, P., McWilliams, J., 1990. Isopycnal mixing in ocean circulation models. J. Phys. Oceanogr. 20, 150–155.
Grooms, I., Majda, A., Smith, K., 2015. Stochastic superparameterization in a quasigeostrophic model of the Antarctic Circumpolar Current. Ocean Modell. 85, 1–15.
Haidvogel, D., Rhines, P., 1983. Waves and circulation driven by oscillatory winds in an idealized ocean basin. Geophys. Astrophys. Fluid Dyn. 25, 1–63.
Herring, J., 1996. Stochastic modeling of turbulent flows. In: Adler, R. et al. (Eds.), Stochastic Modelling in Physical Oceanography. Birkhauser, p. 467.
Ivchenko, V., Sinha, B., Zalesny, V., Marsh, R., Blaker, A., 2013. Influence of bottom topography on integral constraints in zonal flows with parameterized potential vorticity fluxes. J. Phys. Oceanogr. 43, 922–943.
Jansen, M., Held, I., 2014. Parameterizing subgrid-scale eddy effects using energetically consistent backscatter. Ocean Modell. 80, 36–48.
Karabasov, S., Berloff, P., Goloviznin, V., 2009. CABARET in the ocean gyres. Ocean Modell. 30, 155–168.
Kravtsov, S., Kondrashov, D., Ghil, M., 2005. Multi-level regression modeling of nonlinear processes: derivation and applications to climatic variability. J. Clim. 18, 4404–4424.
Li, H., von Storch, J.-S., 2013. On the fluctuating buoyancy fluxes simulated in a 1/10-degree OGCM. J. Phys. Oceanogr. 43, 1270–1287.
Marshall, D., Maddison, J., Berloff, P., 2012. A framework for parameterizing eddy potential vorticity fluxes. J. Phys. Oceanogr. 42, 539–557.
McWilliams, J., 2008. The nature and consequences of oceanic eddies. In: Hecht, M., Hasumi H. (Eds.), Eddy-Resolving Ocean Modeling. AGU Monograph. 131–147.
Penland, C., 2007. Stochastic linear models of nonlinear geosystems. In: Tsonis, A., Elsner, J. (Eds.), Nonlinear Dynamics in Geosystems. Springer, New York, p. 604.
Porta Mana, P., Zanna, L., 2014. Toward a stochastic parameterization of ocean mesoscale eddies. Ocean Modell. 79, 1–20.
Rypina, I., Kamenkovich, I., Berloff, P., Pratt, L., 2012. Eddy-induced particle dispersion in the upper-ocean North Atlantic. J. Phys. Oceanogr. 42, 2206–2228.
Srinivasan, K., Young, W., 2014. Reynolds stress and eddy diffusivity of beta-plane shear flows. J. Phys. Oceanogr. 71, 2169–2185.
Starr, V., 1968. Physics of Negative Viscosity Phenomena. McGraw-Hill, New York (p. 256).
Waterman, S., Jayne, S., 2011. Eddy-mean flow interactions in the along-stream development of a western boundary current jet: an idealized model study. J. Phys. Oceanogr. 41, 682–707.
Waterman, S., Jayne, S., 2012. Eddy-driven recirculations from a localized transient forcing. J. Phys. Oceanogr. 42, 430–447.
Whitehead, J., 1975. Mean flow generated by circulation on a beta-plane: an analogy with the moving flame experiment. Tellus 4, 358–363.